

RESEARCH

Open Access



Eubacterium siraeum suppresses fat deposition via decreasing the tyrosine-mediated PI3K/AKT signaling pathway in high-fat diet-induced obesity

Xueshuang Lai¹, Shuang Liu¹, Jian Miao¹, Ran Shen¹, Zhen Wang¹, Zhe Zhang¹, Huanfa Gong¹, Meng Li³, Yuchun Pan^{1,2*} and Qishan Wang^{1,2*}

Abstract

Background Obesity in humans can lead to chronic diseases such as diabetes and cardiovascular disease. Similarly, subcutaneous fat (SCF) in pigs affects feed utilization, and excessive SCF can reduce the feed efficiency of pigs. Therefore, identifying factors that suppress fat deposition is particularly important. Numerous studies have implicated the gut microbiome in pigs' fat deposition, but research into its suppression remains scarce. The *Lulai black pig* (LL) is a hybrid breed derived from the *Laiwu pig* (LW) and the *Yorkshire pig*, with lower levels of SCF compared to the LW. In this study, we focused on these breeds to identify microbiota that regulate fat deposition. The key questions were: Which microbial populations reduce fat in LL pigs compared to LW pigs, and what is the underlying regulatory mechanism?

Results In this study, we identified four different microbial strains, *Eubacterium siraeum*, *Treponema bryantii*, *Clostridium* sp. CAG:413, and *Jeotgalibaca dankookensis*, prevalent in both LW and LL pigs. Blood metabolome analysis revealed 49 differential metabolites, including tanshinone IIA and royal jelly acid, known for their anti-adipogenic properties. *E. siraeum* was strongly correlated with these metabolites, and its genes and metabolites were enriched in pathways linked to fatty acid degradation, glycerophospholipid, and glycerolipid metabolism. In vivo mouse experiments confirmed that *E. siraeum* metabolites curb weight gain, reduce SCF adipocyte size, increase the number of brown adipocytes, and regulate leptin, IL-6, and insulin secretion. Finally, we found that one important pathway through which *E. siraeum* inhibits fat deposition is by suppressing the phosphorylation of key proteins in the PI3K/AKT signaling pathway through the reduction of tyrosine.

Conclusions We compared LW and LL pigs using fecal metagenomics, metabolomics, and blood metabolomics, identifying *E. siraeum* as a strain linked to fat deposition. Oral administration experiments in mice demonstrated that *E. siraeum* effectively inhibits fat accumulation, primarily through the suppression of the PI3K/AKT signaling pathway, a critical regulator of lipid metabolism. These findings provide a valuable theoretical basis for improving pork quality and offer insights relevant to the study of human obesity and related chronic metabolic diseases.

Keywords *Laiwu pig*, *Lulai black pig*, Fat deposition, *Eubacterium siraeum*

*Correspondence:

Yuchun Pan

panyc@zju.edu.cn

Qishan Wang

wangqishan@zju.edu.cn

Full list of author information is available at the end of the article



© The Author(s) 2024. **Open Access** This article is licensed under a Creative Commons Attribution-NonCommercial-NoDerivatives 4.0 International License, which permits any non-commercial use, sharing, distribution and reproduction in any medium or format, as long as you give appropriate credit to the original author(s) and the source, provide a link to the Creative Commons licence, and indicate if you modified the licensed material. You do not have permission under this licence to share adapted material derived from this article or parts of it. The images or other third party material in this article are included in the article's Creative Commons licence, unless indicated otherwise in a credit line to the material. If material is not included in the article's Creative Commons licence and your intended use is not permitted by statutory regulation or exceeds the permitted use, you will need to obtain permission directly from the copyright holder. To view a copy of this licence, visit <http://creativecommons.org/licenses/by-nc-nd/4.0/>.

Background

Fat deposition is a crucial physiological process for pigs, influencing both muscle and subcutaneous tissues and affecting pork quality. Fat deposited in muscle tissue is known as intramuscular fat (IMF), while fat under the skin is referred to as subcutaneous fat (SCF). An increase in IMF makes the meat more tender, juicy, and flavorful [1]. However, excessive SCF is detrimental as it reduces feed conversion efficiency, prolongs the rearing period, and elevates production costs. Comparisons of cytoplasmic triglycerides in IMF and SCF have shown that SCF cells accumulate more fat than IMF cells, indicating a greater propensity for lipid deposition in SCF [2]. Therefore, finding a method to inhibit SCF while minimizing the impact on IMF would reduce feeding costs without compromising meat quality, addressing a key issue in the pig farming industry. Furthermore, fat deposition is a vital physiological process in humans, and its imbalance can lead to obesity, a precursor to various chronic metabolic diseases, including insulin resistance, hyperlipidemia, hypertension, diabetes, coronary heart disease, gallbladder disease, and certain cancers [3–5]. Identifying factors that suppress fat deposition could provide new methods for the prevention and treatment of these conditions.

Extensive research has predominantly focused on identifying genetic factors influencing fat deposition in pigs, yielding important genes that affect fatness, such as HMGAI, PLAG1, MYH3, TBC1D1, BAAT, and PHLPP1 [6–9]. However, an organism functions as a symbiotic system comprising both the host and its resident microbiota. Alterations in the microbiome or host genome can affect the physiology and adaptability of this symbiotic system, potentially leading to genetic variations within the symbiotic genome [10]. Notably, significant differences in gut microbiome composition have been observed between fat and lean pigs. For instance, *Rongchang* pigs, known for their high fat content, exhibit a higher proportion of Bacteroidetes compared to *Yorkshire* pigs, which are characterized by low fat content [11]. In *Duroc* × *Landrace* × *Yorkshire* (DLY) pigs, *Lactobacillus johnsonii* has been shown to promote lipid deposition and metabolism by altering the gut microbiome [12]. Additionally, *Prevotella copri* has been found to have a significant association with fat accumulation in pigs [13]. Microbial metabolites, such as short-chain fatty acids (SCFAs), are recognized as central messengers between the microbiota and the host, and their dysregulation is implicated in the development of fat deposition [14, 15]. Therefore, Investigating the relationship between gut microbiota, metabolites, and host functions will illuminate potential targets for understanding and managing fat deposition.

Building on our previous work [16], we will utilize multi-omics data from *Laiwu* (LW) and *Lulai black pigs* (LL) to achieve this objective. LW pigs have an average intramuscular fat (IMF) content of 12.78% and an average backfat thickness (measured by subcutaneous fat, SCF) of 41.2 mm. LL pigs, a hybrid breed derived from LW pigs and *Yorkshire pigs* with 50% of their genetic lineage originating from LW pigs [17], exhibit lower IMF and SCF content compared to LW pigs, with an average IMF content of 7% and an average backfat thickness of 34.8 mm [18]. The significant differences in IMF and SCF content and the close genetic relationship between LW and LL pigs suggest a greater likelihood of identifying gut microbiota with the potential to inhibit fat deposition.

In the gut microbiota of LW and LL pigs, we identified the target strain *E. siraeum*. After culturing *E. siraeum* and isolating its secreted metabolites, we administered these metabolites to mice on a high-fat diet. Compared to the control group, the treated mice exhibited reduced body weight and smaller SCF white adipocytes. Additionally, factors related to fat deposition, including proliferation of brown adipocytes, and the secretion of IL-6, insulin, and leptin, were also influenced. The detailed methodology and results of this study are presented in Fig. 1. This study aims to screen factors associated with inhibiting fat deposition, providing insights for preventing SCF deposition in pigs. The research results also provide a theoretical basis for the prevention and treatment of obesity and its related diseases in humans.

Methods

Animal rearing and sample collection

The methods for animal rearing and sample collection in this study followed those detailed in our previous report [16]. Specifically, eight LW and eight LL pigs were provided with the same diet and housed in a similar environment for approximately 2 years. Fecal samples were collected using specialized collection tubes pre-filled with a bacterial DNA protective agent. For each pig, two fecal samples were collected: one for metagenomic analysis and the other for metabolomic analysis. Prior to blood sample collection, the target pigs were fasted for 14 h. Blood samples were collected via the jugular vein using a syringe to obtain 5 ml of blood. The blood was then transferred into tubes containing a coagulant, which were inverted five times to ensure thorough mixing. The blood mixture was allowed to coagulate at room temperature for approximately 1 h. All collected samples were transported to the laboratory on dry ice to preserve their integrity. This study was conducted in accordance with the ethical guidelines of Zhejiang University in Hangzhou, China.

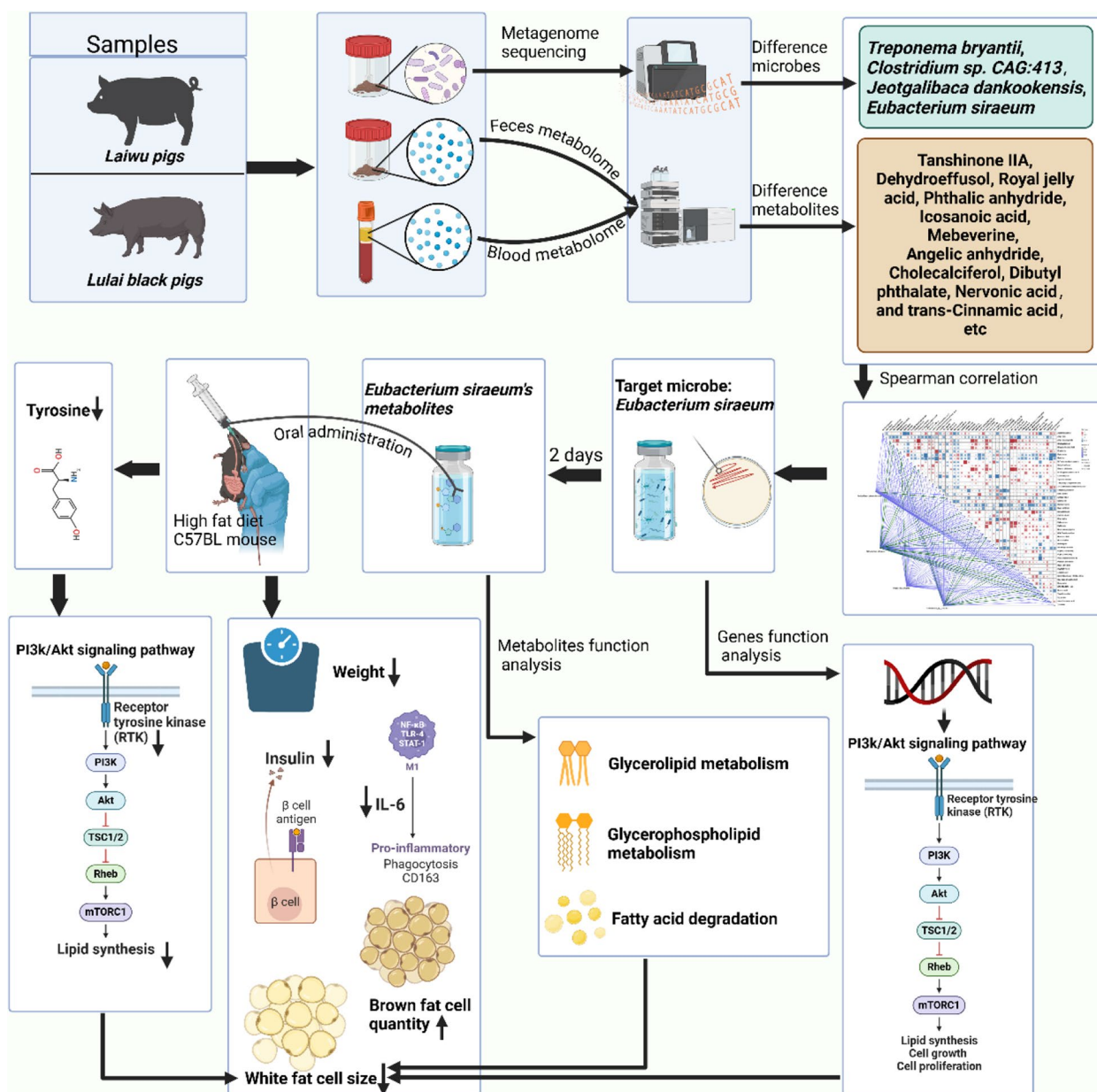


Fig. 1 Study workflow: Four differential microbial strains were found in the fecal microbiota of *Laiwu pigs* and *Lulai black pigs*. Multiple differential metabolites were found in the blood of the two breeds, with tanshinone IIA and royal jelly acid being proven to have anti-adipogenic functions. Correlation analysis revealed that *E. siraeum* was strongly positively correlated with these anti-adipogenic metabolites, leading to its selection as the target microbe for further functional studies. Gene analysis of *E. siraeum* showed its involvement in 161 signaling pathways, including the insulin signaling pathway and the PI3K/AKT signaling pathway. Further investigation of the metabolites secreted by *E. siraeum* revealed their involvement in pathways such as fatty acid degradation. Gavage of high-fat diet mice with *E. siraeum* metabolites resulted in reduced body weight, white adipocyte size, insulin, leptin, and IL-6 secretion, along with an increase in brown fat cells. Overall, *E. siraeum* effectively inhibits fat deposition in mice through multiple mechanisms

Extraction and sequencing of porcine fecal microorganisms

Total genomic DNA from fecal contents was extracted utilizing the E.Z.N.A Soil DNA Isolation kit (OMEGA,

Norcross, GA, USA). DNA quality was assessed using 1% agarose gel electrophoresis and a NanoDrop 2000 Spectrophotometer (Thermo Fisher Scientific, USA). The DNA was then fragmented into 300 bp fragments

employing a Covaris M220 instrument (Qsonica, USA). A paired-end (PE) library was constructed using the TruSeq™ DNA Sample Preparation Kit (Illumina, San Diego, CA). PCR amplification was conducted to enrich the library fragments using the TruSeq PE Cluster Kit v3-cBot-HS (Illumina, San Diego, CA). Subsequent PCR steps generated DNA clusters, and linearization of the DNA amplicons into single strands was achieved. The metagenomic libraries were sequenced on the Illumina NovaSeq6000 platform.

Optimization of porcine metagenomic data processing

The next-generation sequencing (NGS) data was stored in FASTQ format. Sequence trimming was performed using Trimmomatic (v0.39) [19] to ensure high-quality reads. These reads were mapped to the porcine reference genome (Sscrofa 11.1), and reads showing high similarity to the host genome were removed using Burrows-Wheeler Aligner (v0.7.17) [20]. The remaining reads were de novo assembled into contigs using Megahit (v1.1.1) [21]. For open reading frame (ORF) prediction, MetaGeneMark (v3.25) [22] was employed on the assembled contigs, retaining sequences with ORF lengths ≥ 100 bp, which were then translated into amino acid sequences. CD-HIT [23] (<http://www.bioinformatics.org/cd-hit/>) was used for gene sequence clustering, applying 95% identity and 90% coverage as parameters. The longest sequence from each cluster was selected as the representative, forming a non-redundant gene set. High-quality reads from each sample were aligned to this non-redundant gene set using SOAPaligner [24] (<http://soap.genomics.org.cn/>), with 95% identity, and gene abundances were calculated for each sample.

Extraction and detection of metabolites from porcine feces and blood

Feces and blood samples were ground using liquid nitrogen. A 100-mg aliquot of each sample was weighed and mixed with 200 μ l of pre-chilled water and 800 μ l of pre-cooled methanol/acetonitrile (1:1, V/V). The mixture was subjected to ultrasonication in an ice bath for 60 min. Proteins were precipitated at -20 °C for 1 h, followed by centrifugation to obtain the supernatant. The supernatant was dried using a high-speed vacuum centrifuge. For mass spectrum detection, 100 μ l of an acetonitrile–water solution (1:1, V/V) was added for redissolution, followed by centrifugation at 16,000 g at 4 °C for 15 min. The remaining supernatant was separated using the Agilent 1290 Infinity LC high-performance liquid chromatography (UHPLC) system and analyzed with the Triple TOF 5600 mass spectrometer (AB SCIEX). The metabolome raw data were processed for peak alignment, retention time correction, and peak area extraction using XCMS

within the MSDIAL software. Ion peaks with missing values exceeding 50% were excluded. The patterns of all ion peaks were recognized using SIMCA P 14.1 (Umetrics, Umea, Sweden). Metabolite structures were identified through accurate mass number matching (PPM < 25) and second-order spectrogram matching. Standard metabolite databases, including HMDB and MassBank, were consulted to obtain metabolite information.

Eubacterium siraeum culture conditions

Eubacterium siraeum DSM 15702 was cultured for functional validation. The culture medium was composed of peptone (30 g/L), yeast extract (5 g/L), potassium dihydrogen phosphate (5 g/L), glucose (4 g/L), lactose (1 g/L), maltose (1 g/L), soluble starch (1 g/L), crystal violet (0.001 g/L), and L-cysteine (0.5 g/L). The medium was prepared by dissolving 47.5 g of the mixture in 1 L of deionized water. The solution was boiled under a gas mixture of N₂ (80%), H₂ (10%), and CO₂ (10%) and then cooled and adjusted to a pH of 7.0. The medium was dispensed into anaerobic tubes (9 ml per tube) containing 4–5 pebbles, sterilized by autoclaving at 121 °C for 15 min and stored at 4 °C under anaerobic conditions until use.

Functional annotation of the whole genome of *E. siraeum*

The third-generation whole genome sequencing data for the *Eubacterium siraeum* DSM 15702 was sourced from the National Center for Biotechnology Information (NCBI) database under accession number SRR15171276. The genome's open reading frames (ORFs) were predicted using the Prodigal software, and a comparable faa file was generated. The kofam_scan software was utilized for protein sequence homology searches based on HMM models and the kofam database to complete the annotation of gene functions.

Mouse diet

The mouse feed was purchased from Jiangsu Xietong Pharmaceutical Bio-engineering Co., Ltd. The high-fat diet (60% kcal from fat, XTHF60) contains the following ingredients: casein 200 g, L-cystine 3 g, corn starch 0 g, maltodextrin 125 g, sucrose 68.8 g, cellulose 50 g, soybean oil 25 g, mineral mix 10 g, dicalcium phosphate 13 g, calcium carbonate 5.5 g, potassium citrate 16.5 g, vitamin mix 10 g, choline bitartrate 2 g, and significant quantities of lard 245 g, emphasizing its lipid-dense nature. In contrast, the regular diet (10% kcal from fat, XTCON50J) includes casein 200 g, L-cystine 3 g, corn starch 506.2 g, maltodextrin 125 g, sucrose 68.8 g, cellulose 50 g, soybean oil 25 g, lard 20 g, mineral mix 10 g, dicalcium phosphate 13 g, calcium carbonate 5.5 g, potassium citrate 16.5 g, vitamin mix 10 g, and choline bitartrate 2 g,

characteristic of a more balanced caloric distribution. These dietary formulations served as the basis for comparative metabolic and physiological analyses across experimental groups.

Mouse experimental arrangement

In the controlled environment of Zhejiang University's SPF-grade facility, 40 female C57BL/6 J mice, aged 11 weeks, were divided into four experimental groups ($N=10$ per group). The groups were subjected to distinct dietary regimens: the NC group received a standard chow diet, while the NC+*E. siraeum* group was provided the same diet supplemented with *E. siraeum*. Similarly, the HFD group was fed a high-fat diet, while the HFD+*E. siraeum* group had a high-fat diet complemented by *E. siraeum* supplementation. All mice had unrestricted access to food and water. Mice were first acclimated for 1 week, and then those in the *E. siraeum*-treated groups were gavaged with a culture solution containing *E. siraeum* at a concentration of 1×10^9 cfu/ml, administered every 3 days over 2 months, while their counterparts received a control solution devoid of bacteria. Mouse feces were collected at the end of the gavage period. Following a fasting period of 14–16 h, blood, white adipose tissue, and brown adipose tissue were collected for subsequent analysis.

Hematoxylin and eosin (H&E) staining

The histological examination of adipose tissue was undertaken through H&E staining. Samples of both white and brown adipose tissues were fixed in 10% formaldehyde, followed by sequential staining with hematoxylin and eosin. After hematoxylin staining and a water rinse, tissues were treated with 1% hydrochloric acid ethanol, followed by eosin staining. A dehydration sequence in ethanol (80%, 95%, 100%) was applied, culminating in xylene clearing and mounting with Canada balsam. This process enabled the visualization of cellular morphology, critical for assessing tissue-specific responses to dietary and bacterial interventions.

Detection of blood physiological factors in mouse

Fresh blood was stand for 1 h and then centrifuged at a speed of 5000 g for 15 min to separate serum. Aliquots of 200 μ l of the upper serum layer were collected. The serum was temporarily stored in a foam box filled with dry ice and then transported to the laboratory. The concentrations of triglycerides (TG), total cholesterol (TC), spexin, insulin, leptin, and interleukin-6 (IL-6) in the plasma were determined using biochemical assay kits from the Nanjing Jiangcheng Bioengineering Institute.

According to the provided instructions, a mouse TG Elisa assay kit was used to assess TG concentrations, and a mouse TC Elisa assay kit was used to measure TC concentrations. Concentrations of spexin, insulin, leptin, and IL-6 were determined using the respective mouse spexin, insulin, leptin, and IL-6 Elisa assay kit. Each sample was subjected to triplicate analysis, and the absorbance of each well was measured at 450 nm using the Thermo MK3 microplate reader. Standard curves were employed to accurately quantify concentrations, offering insights into the metabolic and inflammatory status of the experimental mice.

Extraction of metabolites from *E. siraeum*, mouse feces, and blood

E. siraeum samples were initially thawed slowly at 4 °C. Mouse feces and blood samples were ground using liquid nitrogen and mixed with 200 μ l of pre-chilled water. A 200- μ l aliquot of all samples was then combined with four times its volume of a pre-chilled methanol/acetonitrile/water solution (2:2:1). The mixture was vortexed for 30 s and subsequently refrigerated at – 20 °C for 1 h to precipitate proteins. The supernatant was separated by centrifugation at 14,000 g for 10 min at 4 °C. The supernatant was transferred to a new Eppendorf tube, vacuum-dried at room temperature, and stored at – 80 °C. Quality control (QC) samples were prepared by mixing the experimental samples in equal volumes, followed by freeze-drying and storage at low temperatures. QC samples were used to evaluate the performance of the instrumentation and to monitor the stability of the chromatography-mass spectrometry system throughout the entire experiment.

Chromatography conditions of *E. siraeum*, mouse feces, and blood metabolites

Metabolite separation was performed using a Nexera UHPLC LC-30A ultra-high-performance liquid chromatography system. The chromatographic column was initially equilibrated with 98% mobile phase A (10 mM ammonium acetate, acetonitrile: water 95: 5, 0.1% formic acid). The sample was then injected into an HILIC column (Waters, ACQUITY UPLC BEH Amide 1.7 μ m, 2.1 \times 100 mm) at a flow rate of 0.3 ml/min. The elution gradient was programmed as follows: 2% mobile phase B (10 mM ammonium acetate, acetonitrile: water 50:50, 0.1% formic acid) for 0.5 min, then increasing to 98% over the next 11.5 min. Mobile phase B was held at 98% for 4 min, after which it was adjusted back to 2% over 0.1 min, followed by a 1.9-min wash.

Mass spectrum conditions of *E. siraeum*, mouse feces, and blood metabolites

The separated metabolites were analyzed using a Q Exactive HF-X mass spectrometer. Positive ion mode detection was employed with a mass scan range of 70–1050 m/z. The first-level mass spectrometry resolution was set to a resolution of 120,000 with an automatic gain control (AGC) target of 3e6 and a maximum ion injection time (IT) of 100 ms. For second-level mass spectrometry, the resolution was set to 7500 with an AGC target of 2e5 and a maximum IT of 50 ms. High-energy collision-induced dissociation (HCD) fragmentation mode was used with normalized collision energy levels set at 20, 40, and 60. The isolation window was 1.5 m/z, and the sub-ion scan range was 200–2000 m/z. In negative ion mode, the mass scan range remained 70–1050 m/z. The first-level mass spectrometry resolution was maintained at 120,000 with an AGC target of 3e6 and a maximum IT of 200 ms. The second-level mass spectrometry resolution was set at 7500 with an AGC target of 2e5 and a maximum IT of 50 ms. Second-level mass spectrometry parameters remained the same, with HCD fragmentation and the same isolation window and sub-ion scan ranges.

Processing of raw data from *E. siraeum*, mouse feces, and blood metabolomics

The raw data (RAW files) of the samples were collected through mass spectrometry. The metabolome data underwent peak alignment, retention time correction, and peak area extraction using Progenesis QI software. Compound identification was comprehensively performed using Metascope, based on criteria such as mass number (PPM < 5), retention time, isotope distribution, fragment ion spectra, and collision cross-section (CCS). Standard metabolite databases, including SDF, HMDB, and MassBank, were consulted to obtain metabolite information.

Statistical analysis

The gene set was aligned against the NR database using Blast (v2.2.28) to retrieve species annotation and abundance data. Blastp was employed to align gene set sequences against the eggNOG database, yielding a Cluster of Orthologous Groups of proteins (COG) information. Microbial species abundance was normalized using TPM. Principal components analysis (PCA) was employed to assess the overall variation and differences between samples in the metagenome. The Kruskal–Wallis rank sum test was used to detect significant differences among all the feature species, with a significance level of $P < 0.05$. The Wilcoxon rank sum test was subsequently conducted to further examine the significant

species identified in the Kruskal–Wallis test, with a significance level of $P < 0.05$. Finally, Linear discriminant analysis (LDA) was then employed to identify the final biomarkers, with an LDA score greater than 2 and a significance level of $P < 0.05$. The variable importance for the projection (VIP) scores was obtained using the OPLS-DA model, which measures the strength and explanatory power of each metabolite's expression pattern for sample classification and discrimination. A threshold of $VIP > 1.0$ was used to determine important metabolites. Spearman correlation analysis was conducted to assess the association between microbes and blood metabolites. The correlation coefficients were interpreted as follows: 0.0–0.2, very weak or no correlation; 0.2–0.4, weak correlation; 0.4–0.6, moderate correlation; 0.6–0.8, strong correlation; and 0.8–1.0, very strong correlation. Significance levels were denoted as follows: $P \geq 0.05$, no label; $0.01 < P < 0.05$, labeled “*”; $0.001 < P < 0.01$, labeled “**”; $P \leq 0.001$, labeled “***”.

Mouse weight and serum physiological factors were compared between the two groups using a *T* test, with differences considered significant at $P < 0.05$. Pathway enrichment analysis identified significantly enriched metabolic and signal transduction pathways, performed using the online platform KOBAS (<http://kobas.cbi.pku.edu.cn>). The relationships between pathways were presented using KEGG network diagrams, which also depicted the associations between metabolites and pathways. Initially, metabolite-enriched pathways were identified through the platform MetaboAnalyst (<https://genap.metaboanalyst.ca/ModuleView.xhtml>). Finally, Cytoscape (v3.10) was utilized to visualize the relationship between metabolites and enriched pathways.

Results

Microbial diversity and composition in LW and LL pig breeds

In this study, we conducted an in-depth exploratory analysis of previously published data [16] to identify key microbial strains involved in regulating fat deposition in LW and LL pigs. The data processing met all necessary requirements and was suitable for further analysis. We performed principal components analysis (PCA) to examine species dispersion. The results indicated that the microbial communities were not entirely distinct between the two pig breeds (Fig. 2a), suggesting more similarities than differences in microbial composition.

According to the annotation information, we quantified the microbial species in the two pig gut microbiomes. LW pigs exhibited a total of 14,570 strains, of which 255 were specific to LW pig. In contrast, LL pigs had a total of 14,324 strains, with only 9 strains specific to LL pigs (Fig. 2b). However, the abundances of these specific

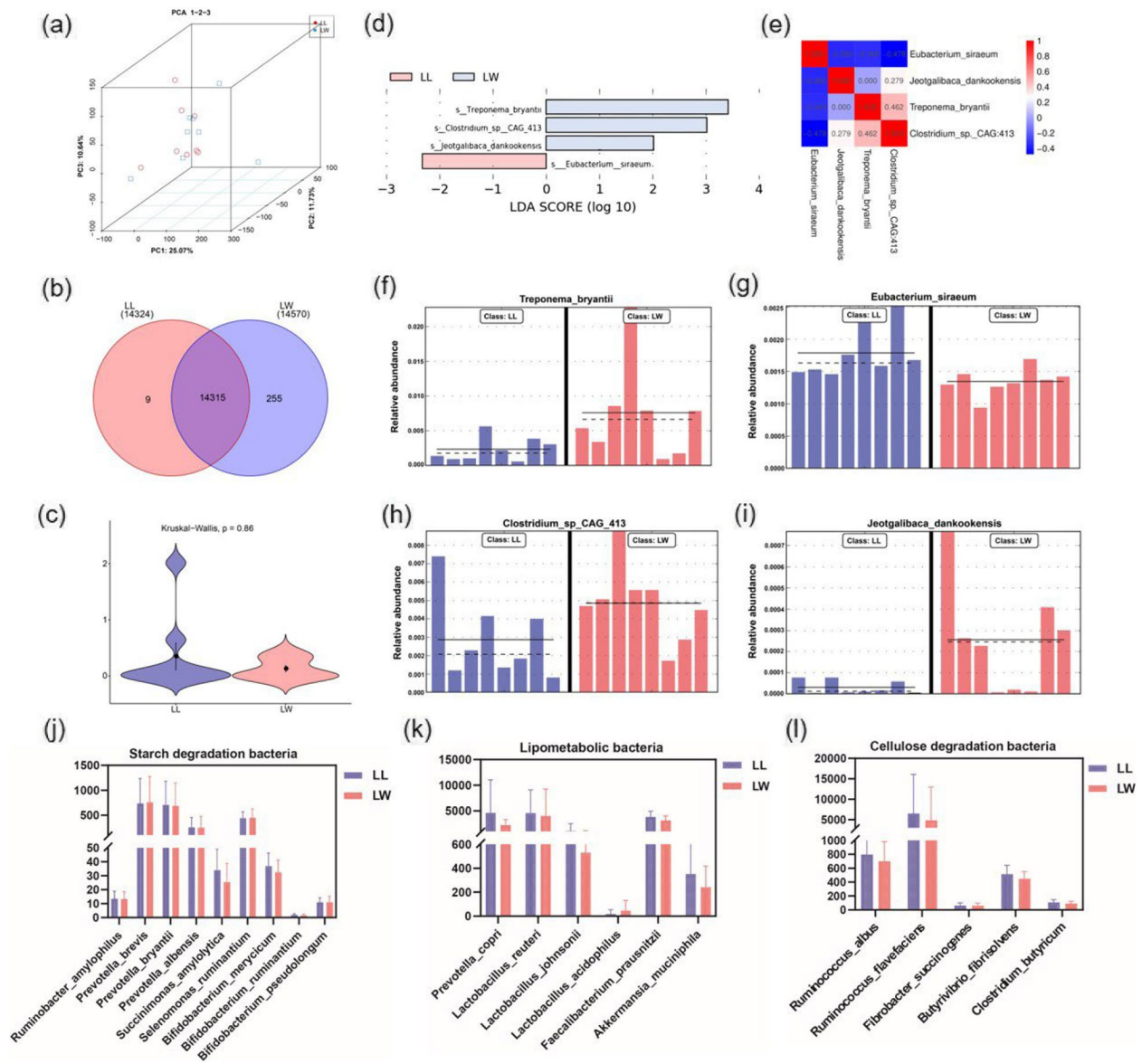


Fig. 2 Analysis of differences in gut microbiota between LW and LL pigs. **a** PCA analysis showed no distinct separation in the microbial classification of the two groups of pigs. **b** A total of 14,315 strains were common to LW and LL pigs. **c** The Kruskal–Wallis rank sum test showed that the significant differences in the two pig microbial communities were not obvious. **d** Linear discriminant analysis identified 4 significantly different microbial strains between the two breeds. **e** Pearson correlation analysis of the four differentiating strains revealed that *E. siraeum* was moderately negatively correlated with *Clostridium* sp. CAG:413. **f–i** The abundance and variation of the four differentiating strains between LW and LL pigs showed that *T. bryantii*, *Clostridium* sp. CAG:413, and *J. dankookensis* were more abundant in LW pigs, while *E. siraeum* was more abundant in LL pigs. **j–l** Abundance of carbohydrate-related and lipometabolic-related strains showed no significant differences between the two pig breeds

strains were very low (CPM < 1), indicating they do not serve as indicative species. Consequently, we identified useful indicator species through differential analysis. First, we used the Kruskal–Wallis test to examine overall differences among the 14,315 microbial strains between the two pig breeds. The results revealed minimal overall difference in the gut microbiota composition (Fig. 2c). Based on the Kruskal–Wallis test (species with $P < 0.05$),

we then conducted a Wilcoxon rank sum test to identify 212 distinct microbial strains with varying abundances between LW and LL pigs (CPM > 1, prevalence > 40%). Of these, 132 strains displayed higher abundance in LW pigs, while 80 strains exhibited higher abundance in LL pigs (Table S1). Notably, three microbial species, namely *T. bryantii*, *Clostridium* sp. CAG:413, and *E. siraeum*, demonstrated abundances exceeding 1000 TPM (Table S1).

Building upon the Wilcoxon rank sum test results (species with $P < 0.05$), we employed linear discriminant analysis (LDA) to further distinguish differentially abundant microbial species between LW and LL pigs. The LDA revealed that four microbial species, including *T. bryantii*, *Clostridium* sp. CAG:413, *E. siraeum*, and *J. dankookensis*, exhibited significant distinctions between the two pig breeds ($P < 0.05$; Fig. 2d, f–i). Among these, *T. bryantii*, *Clostridium* sp. CAG:413, and *J. dankookensis* were significantly enriched in LW pigs, while *E. siraeum* was significantly enriched in LL pigs. Additionally, *T. bryantii*, *Clostridium* sp. CAG:413, and *E. siraeum* showed moderate correlations ($0.4 < |\text{cor}| < 0.6$; Fig. 2e).

We also used the *T* test to identify bacteria involved in starch degradation, lipid metabolism, and cellulose degradation. However, their abundances were comparable between the two pig breeds (Fig. 2j–l). These findings suggest that *T. bryantii*, *Clostridium* sp. CAG:413, *E. siraeum*, and *J. dankookensis* may be important factors influencing the differences in fat deposition between LW and LL pigs.

Functional diversity of clusters of orthologous groups of proteins

Clusters of Orthologous Groups of Proteins (COG) represent protein groups that share a common ancestral origin [25]. Analyzing the protein functions of gut microbiota in LW and LL pigs can provide insights into the functional roles of their distinct microbial communities. In this study, we annotated 28,357 and 25,586 COGs in the gut microbiota of LW and LL pigs, respectively (Fig. S1). These COGs were further categorized into 22 functional classes, with no significant differences observed between the two breeds (Fig. S2).

We then identified 198 differentially abundant COGs, meeting the criteria of CPM > 1 and prevalence > 40%. Among these, 109 COGs were more abundant in LW pigs, while 89 COGs were more abundant in LL pigs (Table S2). Among these, phosphoribosyltransferase (COG2236), glycosyl transferase family 2 (ENOG4110742), phosphatidate cytidyltransferase (COG0170), ABC transporter (COG4143), glycoside hydrolase family 13 (ENOG4111TNM), fructose 1,6-bisphosphatase (EC 3.1.3.11, COG1980) and NADH flavin oxidoreductase (COG1902) were more abundant in LW pigs (Fig. 3a–g). Notably, fructose 1,6-bisphosphatase is a key enzyme in gluconeogenesis, responsible for converting non-carbohydrate substances into glucose [26, 27]. NADH flavin oxidoreductase is involved in energy production and conversion [28]. Conversely, a carrier of the growing fatty acid chain in fatty acid biosynthesis (COG0236), homocysteine S-methyltransferase (COG2040), methionine adenosyltransferase (ENOG410YTXD), peptidyl-arginine deiminase (ENOG4111XJA), pyruvate kinase (COG1751), and family 2

glycosyl transferase (ENOG4110742) was found to be more abundant in LL pigs (Fig. 3h–l). Notably, methionine adenosyltransferase (MAT) plays a crucial role in regulating lipid metabolism, and alterations in methionine metabolism have been associated with weight gain in obese individuals [29]. Pyruvate kinase can inhibit the expression of thermogenic genes in brown adipocytes [30].

E. siraeum is tightly correlated with blood anti-adipogenic metabolites

Metabolites also play crucial roles in fat deposition, regulating various host metabolic processes such as energy homeostasis, glucose metabolism, and lipid metabolism [31–33]. Therefore, we conducted an analysis of microbial and blood metabolites in LW and LL pigs to identify potential markers for fat deposition. The results indicated that three microbial metabolites, including antheraxanthin, 3'-deoxycapsanthin, and bayogenin (VIP > 1, $P < 0.05$), were significantly more abundant in LL than in LW pigs (Fig. 4a). Previous literature has reported that antheraxanthin has antioxidant effects and has not been detected in human blood [34, 35]. Bayogenin can inhibit cancer cell growth and has a targeting effect on hexokinase II (HK2) [36]. 3'-deoxycapsanthin, isolated from capsanthin, has antioxidative properties [37]. However, these microbial metabolites alone do not provide sufficient evidence to act as indicators of fat deposition, prompting us to focus on differential blood metabolites. Using Lefse analysis, we found 49 significantly different blood metabolites between the two pig breeds (score > 2, $P < 0.05$; Fig. 4b; Table S3). Functional enrichment analysis revealed that these metabolites were involved in 12 signaling pathways, with significant enrichment in the biosynthesis of unsaturated fatty acids and the phenylalanine, tyrosine, and tryptophan biosynthesis pathways (Fig. 4c). Within these pathways, stearic acid and icosanoic acid were specially enriched in the biosynthesis of unsaturated fatty acids, while tyrosine exhibited enrichment in the phenylalanine, tyrosine, and tryptophan biosynthesis pathway (Table S4). Literature evidence suggests that stearic acid contributes to the reduction of total fat content and visceral fat content in mice, and lowers serum glucose levels [38], indicating its role in fat deposition differences between LW and LL pigs. Additionally, other blood metabolites such as royal jelly acid have been reported to regulate fat deposition [39, 40]. Furthermore, the microbial metabolites exhibit a strong correlation with these blood metabolites (Fig. 4d; Table S5). Antheraxanthin and 3'-deoxycapsanthin were positively correlated with gomisins H, juarezic acid, and others, suggesting both antioxidant and anti-inflammatory effects. Bayogenin was negatively correlated with stearic acid and appears to inhibit both cancer cell and adipocyte growth.

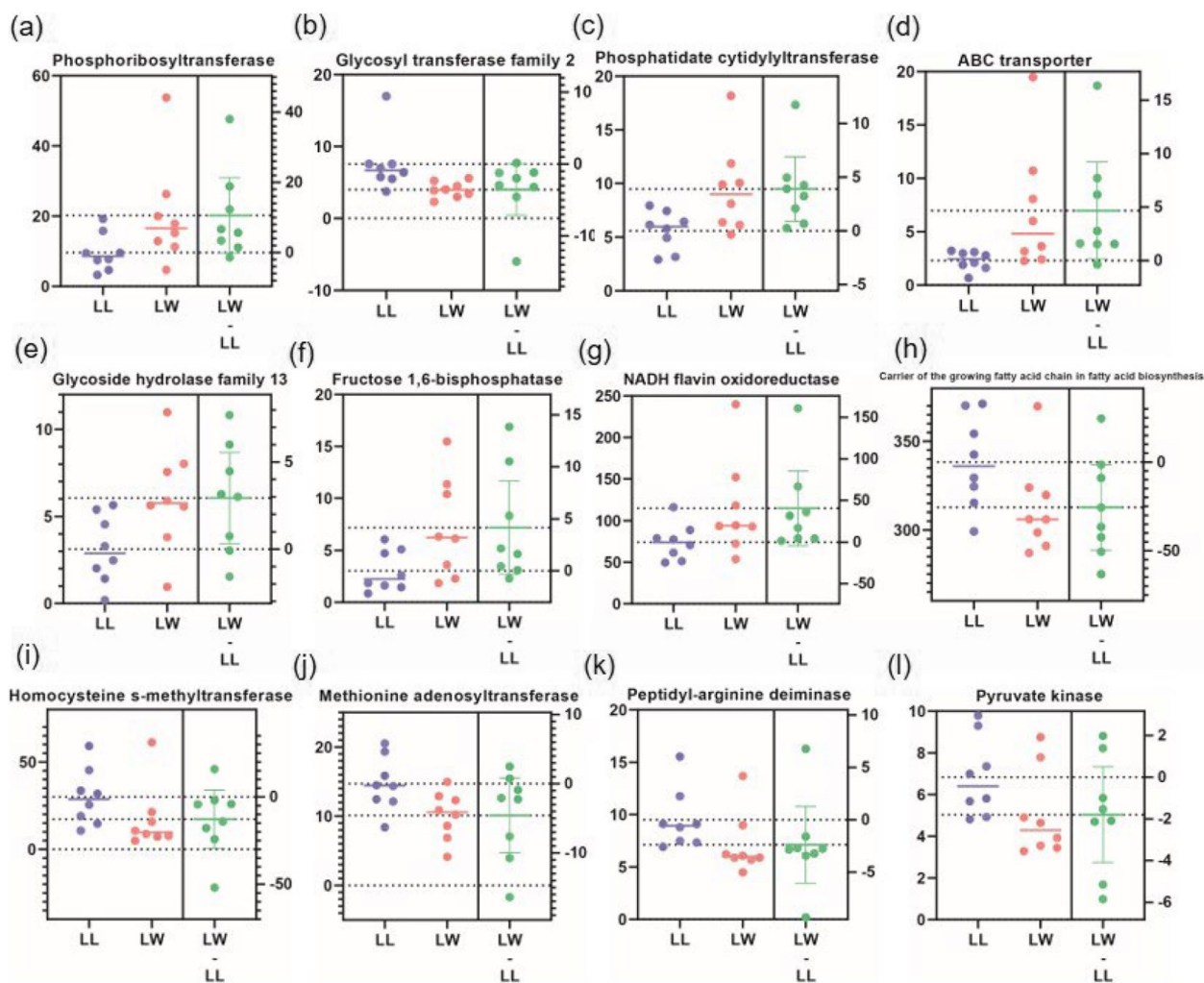


Fig. 3 Differences in Clusters of Orthologous Groups (COGs) related to carbohydrate and lipid metabolism between LW and LL pigs. **a–g** COGs with higher abundance in LW pigs. **h–l** COGs with higher abundance in LL pigs

We further conducted correlation analysis using blood metabolites as markers to identify key microbial species influencing fat deposition. This analysis revealed 196 correlation pairs between the four differential microbial species and the differential blood metabolites, with 33 pairs showing statistically significant correlations (Table S6). Specifically, *E. siraeum* showed a strong positive correlation with several metabolites, including tanshinone IIA, dehydroeffusol, royal jelly acid, phthalic anhydride, icosanoic acid, mebeverine, SPI_256.2273_14.6, angelic anhydride, cholecalciferol, dibutyl phthalate, nervonic acid, and trans-cinnamic acid (Fig. 5a). Conversely, *Clostridium* sp. CAG:413 exhibited strong negative correlations with nervonic acid, tanshinone IIA, phthalic anhydride, and royal jelly acid, opposite to the effects of *E. siraeum*

(Fig. 4e). This suggests that *E. siraeum* may inhibit fat deposition, while *Clostridium* sp. CAG:413 promotes it, given the involvement of tanshinone IIA, royal jelly acid, and nervonic acid in inhibiting fat deposition [39, 41, 42]. *T. bryantii* and *J. dankookensis* exhibited relatively weak correlations with metabolites. *T. bryantii* only showed a strong negative correlation with creatinine, while *J. dankookensis* only exhibited a strong positive correlation with ginkgolide A (Fig. 4e). It is worth noting that *E. siraeum* exhibited the most significant positive correlation with blood differential metabolites, with 18 pairs of correlation, many of which have been demonstrated to inhibit fat deposition. The higher abundance of *E. siraeum* in LL pigs, which have lower fat content, suggests that *E. siraeum* likely plays a key role in inhibiting fat deposition.

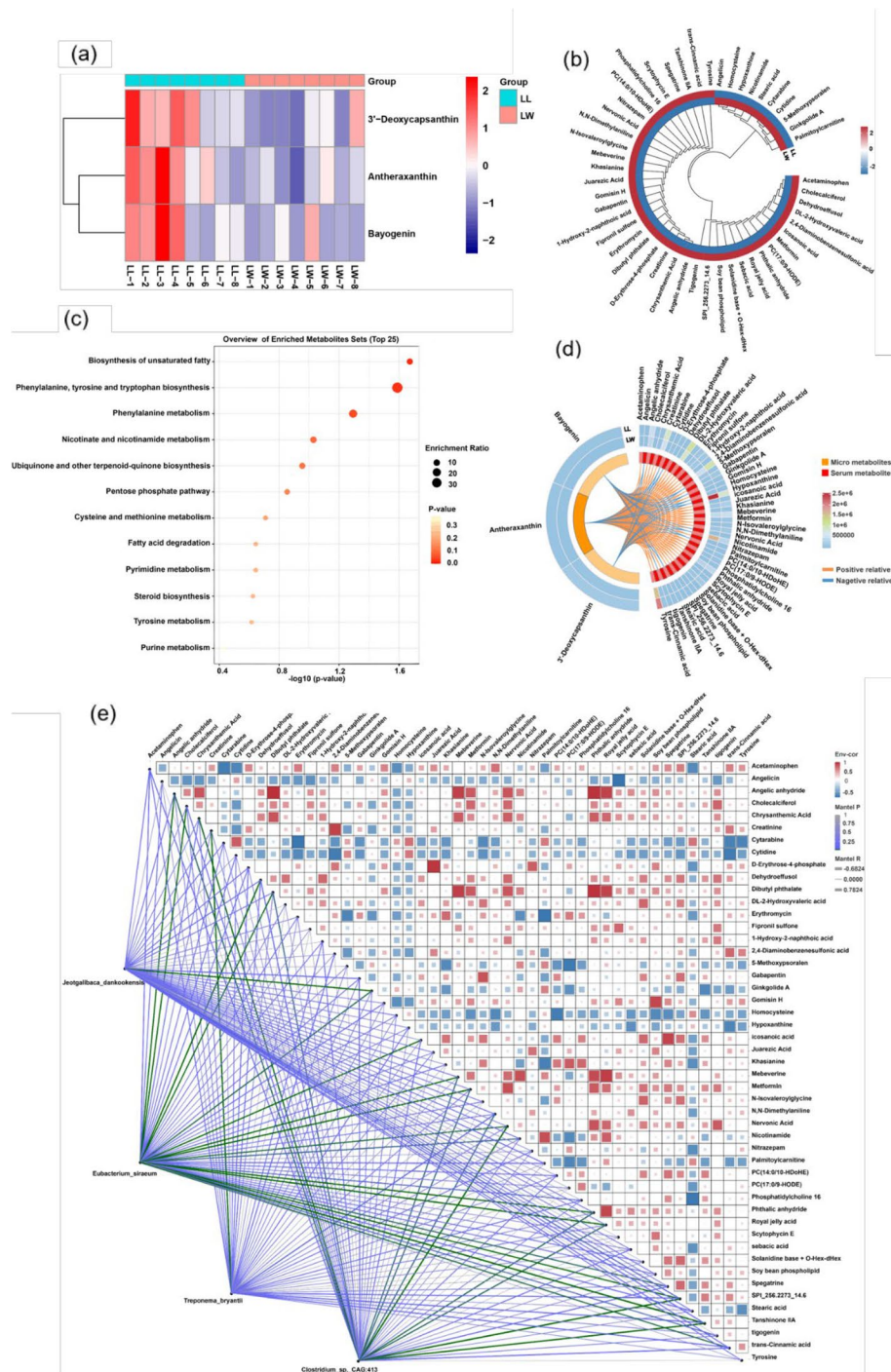


Fig. 4 Differences in microbial and blood metabolites between LW and LL pigs, and pathway enrichment of differential blood metabolites. **a** The 3 differential microbial metabolites. **b** The 49 differential blood metabolites. **c** Enriched pathways of differential blood metabolites. **d** Spearman correlation analysis of the 3 differential micro-metabolites and the 49 differential blood metabolites. **e** Spearman correlation analysis between 4 differential bacteria and the 49 differential blood metabolites, as well as Pearson correlation analysis among differential blood metabolites. Green lines in the bottom left part indicate strong correlations, while purple lines indicate weak or non-correlations. *T. bryantii* and *J. dankookensis* are each strongly associated with only one metabolite. *E. siraenum* exhibits the highest number of strong correlations, with 18 correlated metabolites. The top-right shows correlations between the blood metabolites. The larger the square, the stronger the correlation, with red indicating a positive correlation and blue indicating a negative correlation. Some metabolites display very strong interrelationships

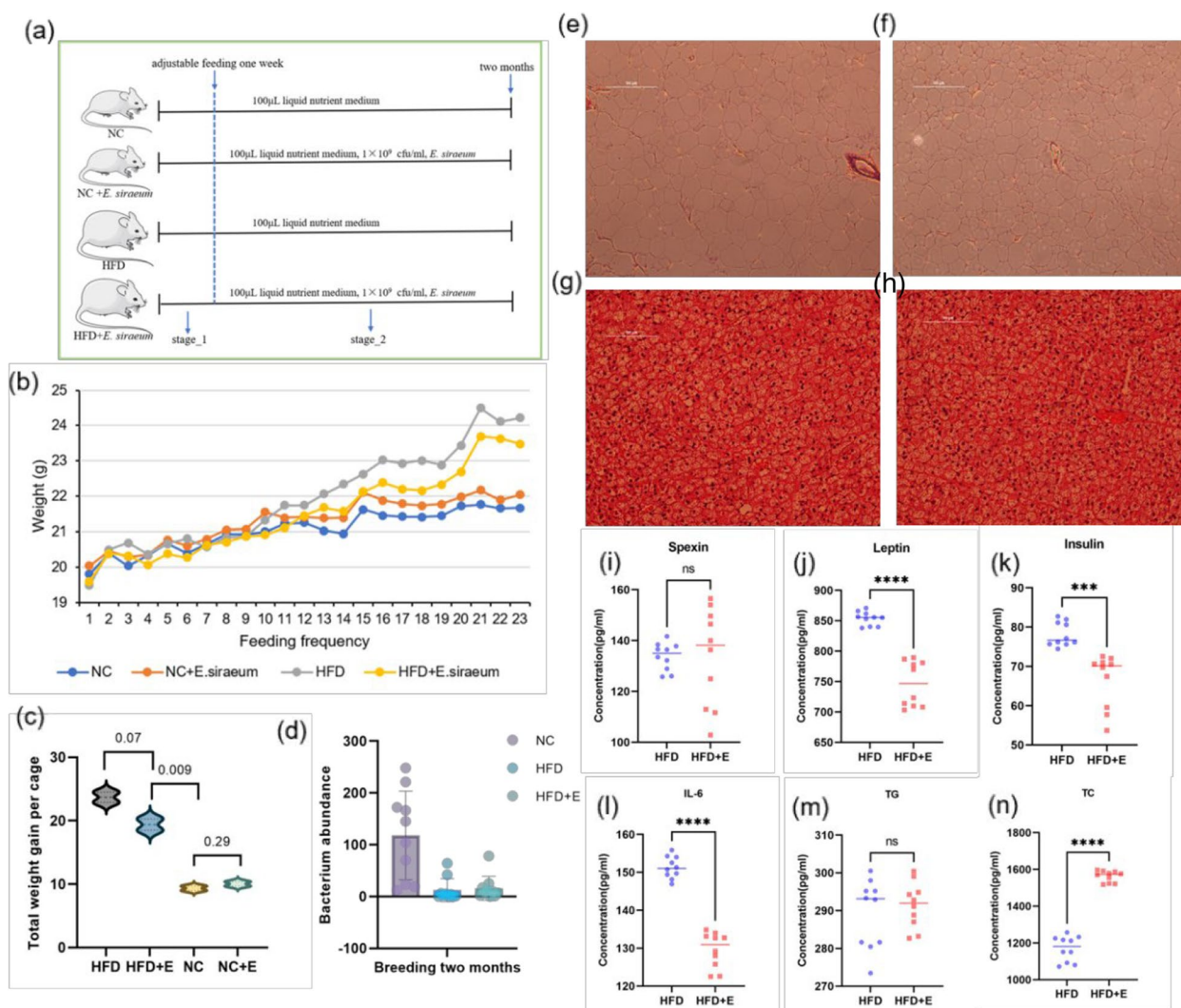


Fig. 5 Changes in various parameters after gavage with *E. siraeum* in high-fat diet mice. **a** Mice were divided into the NC group, NC + E group, HFD group, and HFD + E group. After 1 week of adaptation feeding, each group was orally gavaged with 100 μ l of culture medium every 2 days for 2 months. **b** The weight gain trend of mice in the NC group, NC + E group, HFD group, and HFD + E group during the 2-month feeding period. **c** Post-feeding weight comparisons revealed no significant difference between the HFD and HFD + E groups, though the *p*-value approached 0.07. **d** Comparison of *E. siraeum* colonization in mice between the HFD group and the HFD + E group, with little to no colonization observed compared to the NC group. **e** White adipocyte size in the HFD group. **f** White adipocyte size in the HFD + E group. **g** Number of brown adipocytes in the HFD group. **h** Number of brown adipocytes in the HFD + E group. **i–n** Differences in spexin, leptin, insulin, IL-6, TG, and TC between the HFD and HFD + E groups

Functional enrichment analysis of *E. siraeum* genes

To further investigate the functional roles of *E. siraeum* in host interaction, we conducted a KEGG pathway enrichment analysis of its genes. A total of 161 enriched pathways were identified (Table S7). Among the top enriched gene pathways (Fig. S3), a significant number of genes were found in the biosynthesis of secondary metabolites, totaling 5366 genes. Additionally, several other pathways with thousands of enriched genes included biosynthesis of amino acids (3257 genes),

cysteine and methionine metabolism (1742 genes), carbon metabolism (1521 genes), glucagon signaling pathway (1502 genes), two-component system (1263 genes), starch and sucrose metabolism (1223 genes), glycolysis/gluconeogenesis (1178 genes), insulin signaling pathway (1164 genes), and insulin resistance (1141 genes). Collectively, these pathways account for at least 21% of the total genes in *E. siraeum*.

The large number of genes enriched in the insulin signaling pathway suggests that *E. siraeum* is involved

in regulating the host's insulin sensitivity. Furthermore, *E. siraeum* has a substantial number of genes involved in various aspects of lipid metabolism, energy metabolism, and carbohydrate metabolism, such as glycerolipid metabolism (271 genes) and glycerophospholipid metabolism (219 genes). This indicates that *E. siraeum* may primarily regulate the host's fat deposition by mediating the synthesis and metabolism of glycerolipids and glycerophospholipids. In terms of signal transduction, *E. siraeum* is particularly enriched in the PI3K/AKT, AMPK, and FoxO signaling pathways. These findings suggest that *E. siraeum* may play a central role in regulating the host's diabetes and lipid metabolism-related processes via these pathways.

Validation of *E. siraeum* anti-adipogenic effects through gavage experiments in mice

To verify the anti-adipogenic effects of *E. siraeum*, we conducted a gavage experiment in mice. Mice were divided into four groups: high-fat diet (HFD), negative control (NC), *E. siraeum* administration on a high-fat diet (HFD+E), and *E. siraeum* administration on a normal diet (NC+E), and were monitored over a 2-month feeding period (Fig. 5a). All groups of mice showed an upward trend in weight, with the HFD group exhibiting the fastest increase. The HFD group started with the lightest average weight and ended with the heaviest average weight at the time of sampling (Fig. 5b). In contrast, the HFD+E group had a slower upward trend compared to the HFD group (Fig. 5b), suggesting that the addition of *E. siraeum* can mitigate the rate of weight gain in mice consuming a high-fat, high-calorie diet. Both NC and NC+E groups showed parallel and slow weight increases (Fig. 5b), suggesting that *E. siraeum* does not affect mouse weight under normal diet conditions. When comparing overall weight gain (final minus initial weight), no significant difference was observed between the HFD and HFD+E groups; however, the trend approached significance ($P=0.07$) (Fig. 5c). There was a significant difference between the mice on a high-fat diet and those on a normal chow diet ($P<0.009$). No significant difference was observed between the NC and NC+E groups ($P=0.29$; Fig. 5c).

We then compared the size of white adipocytes and the number of brown adipocytes between the HFD and HFD+E groups. The results showed that white adipocytes in the HFD+E group were smaller in volume compared to the HFD group (Fig. 5e–f). Moreover, the HFD+E group exhibited a greater number of brown adipocytes (Fig. 5g–h). We also compared the levels of various biomarkers, including spexin, insulin, leptin, interleukin-6 (IL-6), triglycerides (TG), and total

cholesterol (TC) between the HFD and HFD+E groups. Spexin levels fluctuated widely in the HFD+E group, while they were more stable in the HFD group (Fig. 5i). Insulin levels were significantly lower in the HFD+E group (Fig. 5k), indicating improved insulin sensitivity, consistent with the functional characterization of the *E. siraeum* genome showing involvement in the insulin signaling pathway. Furthermore, decreased insulin secretion corresponds to reduced uptake and storage of fatty acids in adipocytes, thereby inhibiting fat deposition [43]. Leptin levels were also significantly lower in the HFD+E group (Fig. 5j). Since leptin is primarily produced by adipocytes, its secretion decreases with reduced fat mass [44]. The decreased secretion of leptin aligns with the reduction in white adipocyte size (Fig. 5f). IL-6, a marker of inflammation associated with obesity [45], was also significantly reduced in the HFD+E group (Fig. 5l). Interestingly, while triglyceride levels showed no significant difference between the two groups (Fig. 5m), total cholesterol (TC) was significantly higher in the HFD+E group (Fig. 5n). This unexpected result warrants further investigation into the specific metabolic pathways through which *E. siraeum* affects lipid metabolism.

Using 16S rRNA sequencing, we compared the absolute colonization abundance of *E. siraeum* in the HFD, HFD+E, and NC groups. The NC group had colonization of *E. siraeum*, while the HFD and HFD+E groups had almost no colonization (Fig. 5d). This suggests that long-term high-fat feeding can lead to metabolic disruption, creating an unfavorable internal environment for the colonization and growth of *E. siraeum*. Even with timely and adequate supplementation, the disrupted environment still hinders the colonization of *E. siraeum*. Interestingly, despite the lack of colonization, the high-fat-induced weight gain in the HFD+E group was still suppressed. During the gavage process, we also administered a culture medium to the mice. The culture medium contained *E. siraeum* metabolites, while the blank culture medium was devoid of bacterial metabolites. This suggests that it is the metabolites of *E. siraeum* that inhibit fat deposition in mice.

Functional enrichment analysis of metabolites secreted by *E. siraeum*

We detected the metabolites secreted by *E. siraeum*, identifying 1565 metabolites using mass spectrometry in both positive and negative ion modes (Fig. S4; Table S8). Among these metabolites, we identified components such as hypoxanthine, betaine, creatine, glutamic acid, and acetylcholine. According to the Human Metabolome Database (hmdb.ca), these metabolites have biological locations in adipose tissue. Metabolites such as

γ -aminobutyric acid, melatonin, 5-hydroxyindoleacetate, tyramine, tryptamine, indole, and cytosine have biological locations in neurons and nerve cells.

Functional enrichment analysis of the metabolites secreted by *E. siraeum* revealed their involvement in key metabolic pathways, including aminoacyl-tRNA biosynthesis, tryptophan metabolism, arginine and proline metabolism, vitamin B6 metabolism, and histidine metabolism (Fig. S5). These metabolites also play critical roles in the metabolism of 19 amino acids, including 11 non-essential amino acids (arginine, histidine, cysteine, glycine, alanine, proline, tyrosine, serine, aspartate, glutamine, glutamate) and 8 essential amino acids (lysine, tryptophan, phenylalanine, methionine, threonine, isoleucine, leucine, and valine). This suggests that *E. siraeum* not only provides essential amino acids to the host but also supports the metabolism of non-essential amino acids. Some metabolites of *E. siraeum* are also involved in lipid metabolism processes such as fatty acid degradation, glycerophospholipid metabolism, and glycerolipid metabolism, as well as carbohydrate metabolism, including fructose and mannose metabolism, citrate cycle, butanoate metabolism, pentose phosphate pathway, glycolysis/gluconeogenesis, and pentose and glucuronate interconversions. These functional enrichment results align with the functional analysis of *E. siraeum* genes, highlighting its role in regulating host lipid and carbohydrate metabolism through a mutualistic symbiotic process.

Furthermore, a co-expression network of *E. siraeum* metabolites and their associated pathways identified a core network of tightly linked metabolites, such as 1-methylguanine, which regulates the AMPK signaling pathway and influences fatty acid biosynthesis, the insulin signaling pathway, and the PI3K/AKT pathway (Fig. S6).

Oral administration of *E. siraeum* significantly reduces tyrosine levels

Fecal metabolites serve as a crucial link in the gut microbiome's regulation of host physiology. We detected 1,234 metabolites in the fecal samples of both HFD and HFD+E mice, with OPLS-DA score analysis revealing significant differences between the two groups (Fig. S7). Using a threshold of $VIP > 1$ and $\log_2(FC) > 1$, we identified 29 differentially abundant metabolites, including 27 that were significantly

downregulated in the HFD+E group compared to the HFD group, such as tyrosine, N-desmethyltramadol, and N, N-diethylethanolamine. Conversely, tryptamine and DL-glutamine were significantly upregulated in the HFD+E group ($P < 0.05$; Fig. 6a; Table S9).

Functional enrichment analysis of these differential metabolites revealed no significantly upregulated pathways but identified four significantly downregulated metabolic pathways: histidine metabolism, phenylalanine, tyrosine and tryptophan biosynthesis, ubiquinone, and other terpenoid-quinone biosynthesis, and phenylalanine metabolism (Fig. S8). These findings suggest that *E. siraeum* degrade and inhibit metabolites such as tyrosine in the gut while promoting the synthesis of tryptamine and DL-glutamine. Blood metabolite analysis identified 534 metabolites in the positive ion mode and 527 in the negative ion mode. Using OPLS-DA and T-tests with the same thresholds ($VIP > 1$, $\log_2(FC) > 1$), 72 metabolites were upregulated and 176 were downregulated ($P < 0.05$; Fig. 6b; Table S10). Tyrosine was the only metabolite consistently identified in both fecal and blood metabolite pools, indicating its transport from the gut into the bloodstream after *E. siraeum* administration. Further investigation of fecal tyrosine levels in the HFD, HFD+E, and NC groups showed a positive correlation between tyrosine levels and body weight (Fig. 6c). In the blood, tyrosine levels increased with body weight in both HFD and HFD+E mice, though no significant difference was observed between the HFD+E and NC groups (Fig. 6d). These results suggest that high-fat diets elevate tyrosine levels, but *E. siraeum* can mitigate this effect, primarily through inhibition of tyrosine synthesis. The significant reduction in tyrosine levels in both fecal and blood samples from HFD+E mice highlights the key role of *E. siraeum* in metabolite regulation.

Oral administration of *E. siraeum* inhibited the PI3K/AKT signaling pathway

The circulatory system is a critical system for maintaining life and homeostasis. Within the upregulated blood metabolites, we identified six components belonging to lipids and lipid-like molecules (Fig. 7a). Specifically, one metabolite was classified as linoleic acids and derivatives (Fig. 7b). The upregulated metabolites were enriched in pathways associated with the digestion of dietary lipids,

(See figure on next page.)

Fig. 6 Changes in fecal and blood metabolites following oral administration of *E. siraeum* in mice. **a** In fecal samples, 29 differential metabolites were identified, including 27 that were significantly downregulated in the HFD+E group compared to the HFD group, such as tyrosine, while tryptamine and DL-glutamine were significantly upregulated. **b** In blood samples, 248 differential metabolites were identified, with 176 significantly downregulated and 72 upregulated in the HFD+E group compared to the HFD group. **c** Fecal tyrosine levels increased proportionally with body weight in NC, HFD+E, and HFD mice. **d** Blood tyrosine levels showed no significant difference between NC and HFD+E mice, but increased with body weight in HFD+E and HFD mice

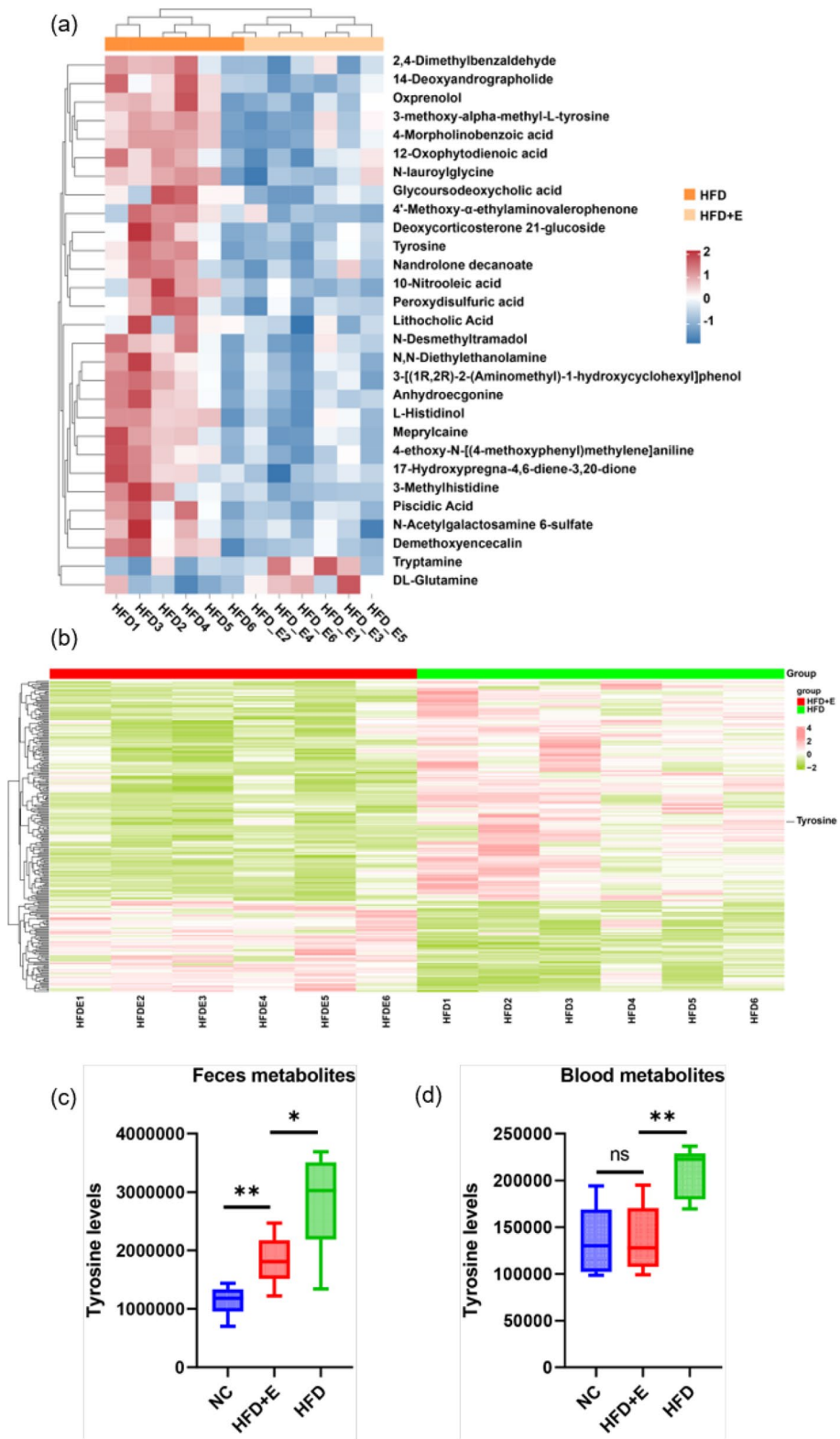


Fig. 6 (See legend on previous page.)

glycerolipid metabolism, triglyceride catabolism, as well as the synthesis of triacylglycerides and triglycerides (Fig. 7e). Importantly, the administration of *E. siraeum* also triggered CYP2E1 reactions, which are known to induce browning in 3T3-L1 white adipocytes [46]. This result is consistent with the increased number of brown adipocytes in mice (Fig. 5h). Additionally, CYP2E1 is involved in drug metabolism and the synthesis of lipids like cholesterol and steroids [47]. Indeed, blood factor testing indicated an increase in total cholesterol (TC) (Fig. 5n). Cholesterol and steroids serve as primary raw materials for thyroid hormones and adrenal cortex hormones. Accordingly, we observed alterations in the production of thyroid hormones and downstream signaling effects in the periphery following inoculation (Fig. 7e). Changes in the effects of PIP2 hydrolysis were also observed in the upregulated pathways. PIP2 can be phosphorylated by PI3K to generate PIP3, which participates in the PI3K/AKT signaling pathway, regulating various aspects of cell activities such as survival, proliferation, growth, and metabolism [48]. Therefore, the hydrolysis of PIP2 is expected to inhibit the function of the PI3K/AKT signaling pathway. In other words, the upregulated metabolites can suppress the PI3K/AKT signaling pathway. A pathway analysis revealed that PIP2 hydrolysis is closely linked to triglyceride catabolism, triglyceride biosynthesis, and dietary lipid digestion, forming an interconnected pathway network (Fig. 7g). This suggests that PIP2 hydrolysis may reduce fat deposition by influencing triglyceride metabolism. Among the 176 downregulated metabolites, 31 components belonged to lipids and lipid-like molecules (Fig. 7c). These substances mainly included fatty acid esters, steroid esters, triterpenoids, diterpenoids, fatty acids and conjugates, and glycerophosphocholines (Fig. 7d). The specific downregulated metabolites can be found in Supplementary Table S10. Functional enrichment analysis of the downregulated metabolites revealed significant involvement in pathways such as aberrant PI3K signaling in cancer and the PI3K/AKT pathway (Fig. 7f), further supporting the inhibitory effect of *E. siraeum* on the PI3K/AKT pathway. The co-expression network of downregulated pathways was divided into three major modules: one related to the PI3K/AKT signaling pathway, another focus on bile acid biosynthesis, and a third involving lysine metabolism and

hyperlysinemia (Fig. 7h). Interestingly, the PI3K/AKT pathway was implicated in both the upregulated and downregulated metabolite pathways, reinforcing its central role in the physiological changes observed following *E. siraeum* administration.

E. siraeum regulates fat deposition through the PI3K/AKT signaling pathway

To elucidate the mechanisms by which *E. siraeum* regulates fat deposition, we integrated data from case–control experiments and literature to outline the pathway involving the PI3K/AKT signaling cascade (Fig. 8). In mice treated with *E. siraeum*, there was a notable increase in PIP2 hydrolysis (Fig. 7g) alongside a marked reduction in the activity of the PI3K/AKT signaling pathway (Fig. 7h). The autophosphorylation of receptor tyrosine kinases (RTKs) in the PI3K/AKT pathway requires ATP to provide the phosphate group, and this ATP–ADP conversion relies on tyrosine as a cofactor. Consequently, a reduction in tyrosine concentration lowers the autophosphorylation levels of RTKs [49, 50]. Our findings revealed that tyrosine levels were significantly reduced in both fecal and blood metabolites of HFD+E mice compared to HFD mice (Fig. 6c–d; Table S9; Table S10). This confirmed that the reduction in tyrosine level in HFD+E mice lowered the phosphorylation level of RTKs, leading to a decrease in the activity of the PI3K/AKT signaling pathway in their white fat tissues (Fig. 8). Additionally, genomic analysis of *E. siraeum* identified 221 genes involved in the PI3K/AKT signaling pathway (Fig. S3), further underscoring the importance of this pathway in *E. siraeum*'s functional repertoire. Furthermore, functional enrichment analysis of metabolites secreted by *E. siraeum* revealed a significant involvement in phenylalanine, tyrosine, and tryptophan biosynthesis (Fig. S5), suggesting that *E. siraeum* metabolites are intricately involved in the regulation of tyrosine synthesis and metabolism.

Discussion

Subcutaneous fat (SCF) deposition negatively impacts feed conversion efficiency in pigs, leading to increased farming costs. Reducing SCF is crucial for enhancing efficiency, and identifying factors that inhibit fat deposition is an important step toward this goal. Previous

(See figure on next page.)

Fig. 7 Functional analysis of blood metabolites in mice. **a** Classification of upregulated metabolites, of which 6 metabolites belong to the lipids and lipid-like molecules category. **b** Lipid categories within the upregulated metabolites. **c** Classification of downregulated metabolites, of which 31 metabolites belong to the lipids and lipid-like molecules category. **d** Lipid categories within the downregulated metabolites. **e** Functional pathways enriched among upregulated metabolites. **f** Functional pathways Enriched among downregulated metabolites. **g** Network of functional pathways related to upregulated metabolites. **h** Network of functional pathways related to downregulated metabolites

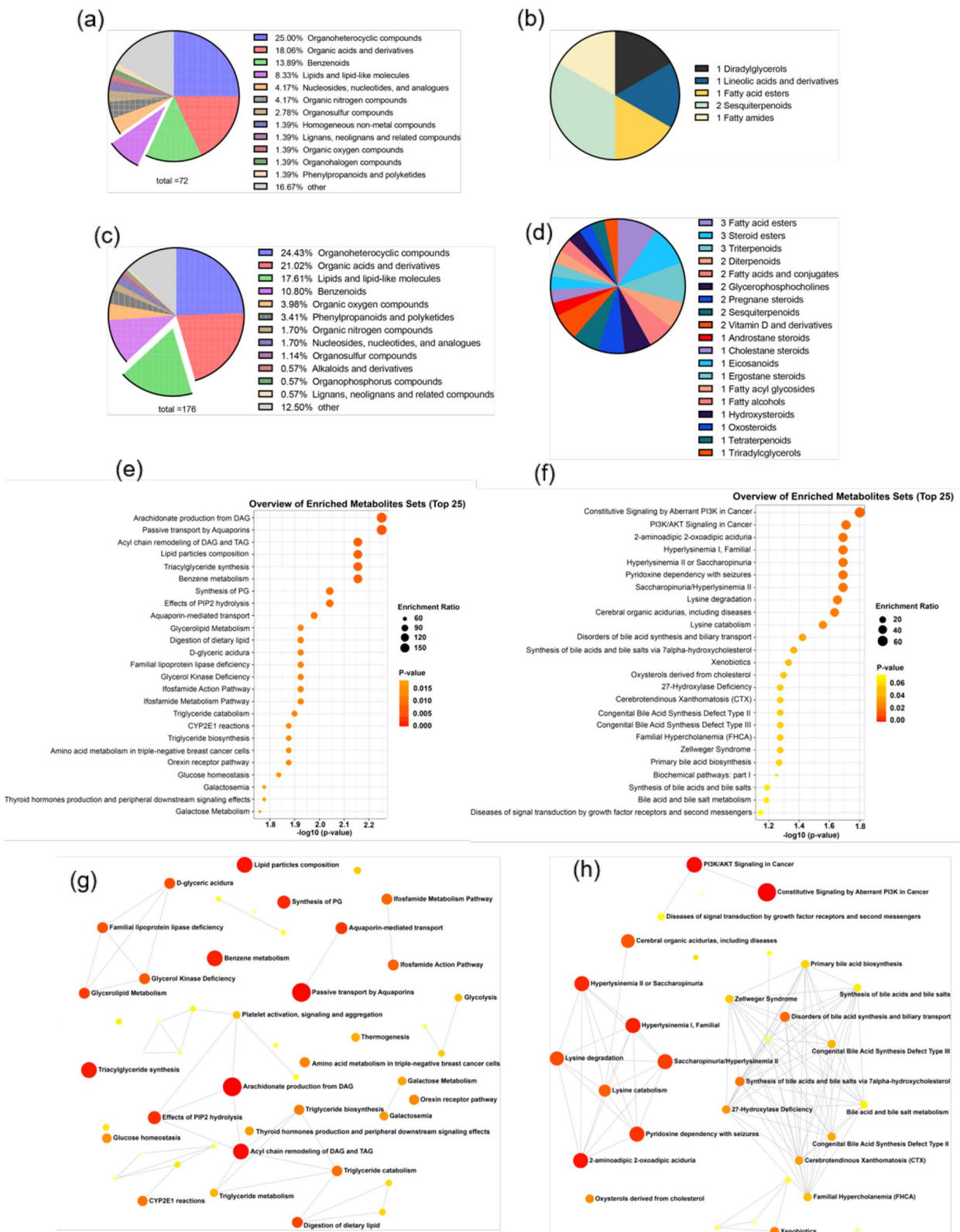


Fig. 7 (See legend on previous page.)

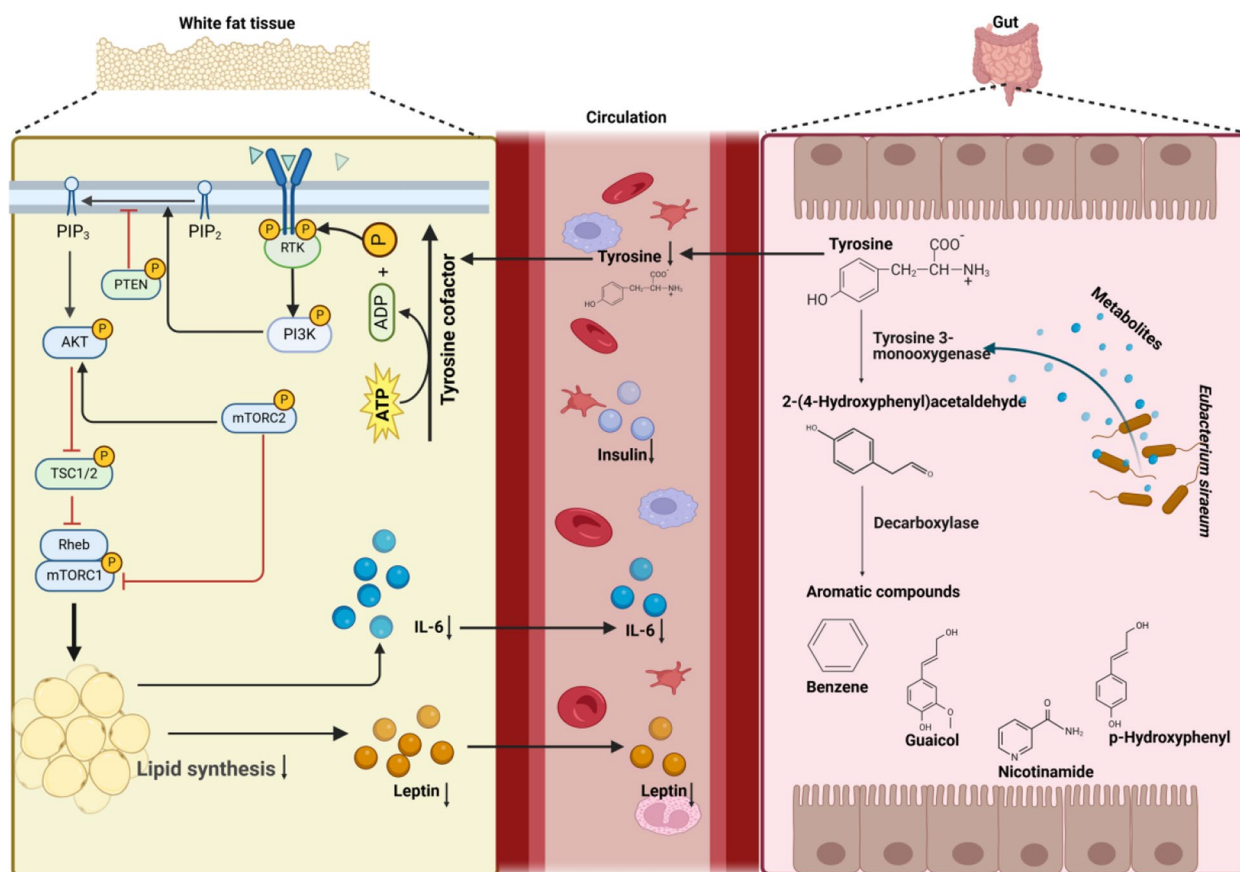


Fig. 8 Pathways through which *E. siraeum* regulates fat deposition. *E. siraeum* reduces fecal tyrosine levels in mice, consequently decreasing blood tyrosine levels. Tyrosine acts as a cofactor in the ATP-ADP conversion reaction, providing phosphate groups to receptor tyrosine kinases (RTKs). Reduced tyrosine levels diminish the phosphorylation level of RTKs, subsequently reducing phosphorylation of the PI3K-AKT pathway and mTORC1. This ultimately leads to a decrease in mRNA transcription levels and lipid synthesis in fat adipocytes. As white adipose tissue is responsible for secreting leptin and the inflammatory cytokine IL-6, the suppression of white adipose tissue results in a corresponding decrease in leptin and IL-6 levels

research has largely focused on the genetic factors influencing fat deposition in pigs [6–9]. This study provides novel insights into the role of *E. siraeum* in regulating fat deposition and metabolic health. By comparing the gut microbiota of LW pigs and LL pigs, we identified *E. siraeum* as a key bacterial strain associated with reduced fat accumulation. *E. siraeum* is known for its anti-inflammatory properties and acetate production [51]. In addition, *E. siraeum* harbors RNA-guided CRISPR effectors such as EsCas13d and EsCas12f1 [52–54]. Compared to obese individuals, *E. siraeum* is predominantly enriched in healthy control groups [55]. In contrast, *Prevotella copri* has been shown to promote fat deposition [13]. Studies in non-human primates on a Mediterranean diet revealed a higher abundance of *P. copri* and a lower proportion of *E. siraeum* when switched to a Western diet [56]. Additionally, pregnant women with normal glucose tolerance (NGT) exhibited a higher abundance of *E. siraeum* than those with gestational diabetes [57]. Supplementation

with *E. siraeum* has been shown to mitigate colitis, along with increases in folate and methylation regulators in the colon [58]. Notably, *E. siraeum* is significantly positively correlated with ethanolamine [59], a metabolite linked to acute coronary syndrome treatment, and plays a role in gut dysbiosis improvement when co-administered with *Bacteroides uniformis* [51]. It is also associated with the regulation of immunoglobulin levels [60].

Our study revealed that *E. siraeum* encodes genes involved in fatty acid degradation, glycerophospholipid metabolism, glycerolipid metabolism, and insulin signaling pathway. These findings suggest that *E. siraeum*, within a mutualistic symbiotic relationship with the host, facilitates fat and lipid degradation via its gene products and metabolites. This might explain its enrichment in lean and healthy populations [55]. Moreover, *E. siraeum* may improve insulin sensitivity, as evidenced by its higher abundance in NGT individuals [57]. A significant number of *E. siraeum*-encoded genes also were

found associated with the biosynthesis of secondary metabolites. Microbial secondary metabolites, such as short-chain fatty acids (SCFAs), are known to modulate nutrient absorption, energy balance, and metabolism in the host [61, 62]. The enrichment of this pathway in *E. siraeum* suggests its contribution to host metabolic regulation, including processes like inflammation, glucose and lipid metabolism, and energy homeostasis. Previous research has confirmed that *E. siraeum* can produce acetate, which plays a role in adipose tissue browning, promoting fat oxidation and increasing brown adipose tissue (BAT) activation [63, 64]. Our findings also demonstrate that oral administration of *E. siraeum* increases brown adipocytes in mice.

In our experiments, we confirmed that *E. siraeum* reduces body weight, decreases SCF white adipocyte size, increases brown adipocytes, lowers leptin and IL-6 secretion, and improves insulin sensitivity in mice. Reduction in white adipocyte size is associated with the breakdown of triglycerides into fatty acids [65]. Brown adipocytes, rich in mitochondria and UCP1 protein, generate heat through non-shivering thermogenesis, a process involving stored fat breakdown into fatty acids [66]. Thus, *E. siraeum* enhances energy expenditure, accelerating lipid degradation in adipocytes. Furthermore, *E. siraeum* promotes the increase of six types of lipids and lipid-like molecules. Conjugated linoleic acids have been shown to have beneficial effects, such as reducing blood lipids, preventing cardiovascular diseases, and assisting in the treatment of diabetes [67]. Another metabolite belonged to guaiane-type sesquiterpenoids, known for their inhibitory effects on validation factors such as TNF- α and IL-6 [68–70]. Melinamide, another upregulated metabolite, has demonstrated the ability to lower cholesterol levels [71, 72]. Overall, *E. siraeum* has the potential to improve the physiological and metabolic environment.

We observed a significant reduction in tyrosine levels following the administration of *E. siraeum*. Previous studies have shown that *E. siraeum* can degrade tyrosine, utilizing it as a carbon and nitrogen source for growth [73–75]. Tyrosine, as a cofactor, facilitates the conversion of ATP to ADP, and the energy release from this conversion is an important condition for the phosphorylation of RTKs [49, 50]. The phosphorylation of RTKs triggers a series of signaling events, including the ERK and PI3K/AKT signaling pathways. On the cell membrane, AKT is phosphorylated and activated, initiating the phosphorylation of multiple substrates, such as TSC1 and TSC2, which are involved in the activation of mTORC1, thereby mediating mRNA translation, protein synthesis, and lipid synthesis [76]. These events typically involve the activation of intracellular signaling pathways that regulate processes such as cell growth, differentiation, survival, and

lipid synthesis [77, 78]. Therefore, a decrease in tyrosine content will inevitably weaken the activity of the PI3K/AKT signaling pathway. Our results demonstrate that both the genes and metabolites of *E. siraeum* participate in the PI3K/AKT pathway, and that this pathway is attenuated in HFD mice following *E. siraeum* administration. This suggests that *E. siraeum* can suppress the PI3K/AKT signaling pathway by reducing tyrosine levels, thus inhibiting lipid synthesis in adipocytes. Previous studies have emphasized the importance of the PI3K/AKT pathway in regulating intramuscular and SCF in pigs [79–81]. Differential expression of mRNAs, including *AKT2*, a key regulatory gene in the fat deposition network, further highlights the relevance of this pathway in fat metabolism [81].

Overall, the process of lipid reduction mediated by *E. siraeum* metabolites involves a complex mechanism that requires the coordination of multiple components and pathways. Within this intricate network, one important mechanism of *E. siraeum* is to lower the levels of tyrosine, suppress the effects of the PI3K/AKT signaling pathway, inhibit lipid synthesis, and ultimately reduce fat deposition in the white adipocytes. Future studies should focus on leveraging *E. siraeum* metabolites to reduce SCF deposition while minimizing impacts on intramuscular fat, balancing both growth and pork quality to meet consumer demands while lowering breeding costs.

Conclusion

In conclusion, we identified *Eubacterium siraeum* as a strain associated with fat deposition in LW and LL pigs. Our experiments using oral administration in mice demonstrated that *E. siraeum* significantly inhibits fat accumulation. This inhibitory effect is largely mediated by the suppression of the PI3K/AKT signaling pathway, a key regulator of lipid metabolism. These findings provide a strong theoretical foundation for improving pork quality through microbiome manipulation and offer valuable insights for future research on human obesity and related metabolic disorders.

Supplementary Information

The online version contains supplementary material available at <https://doi.org/10.1186/s40168-024-01944-4>.

Supplementary Material 1: Figure S1. A total of 28,357 COGs were annotated in the metagenome of Laiwu pigs, and 25,586 COGs were annotated in the metagenome of Lulai black pigs. Among them, 3,530 COGs were specific to Laiwu pigs, 759 COGs were specific to Lulai black pigs, and 24,827 COGs were found in both Laiwu pigs and Lulai black pigs. Figure S2. The COGs annotated in the metagenomes of Laiwu pigs and Lulai black pigs can be categorized into 22 functional classes, and no significant differences were observed. Figure S3. Enriched pathways of genes encoded by *Eubacterium siraeum*, where the numbers on the x-axis represent the quantity of genes enriched in each pathway. Based on the

number of genes in each pathway, revealed a significant enrichment of *E. siraeum* genes in signal transduction, lipid metabolism, energy metabolism, endocrine system, endocrine and metabolic disease, cardiovascular disease, carbohydrate metabolism, and amino acid metabolism. Figure S4. The upper panel shows the mass spectrum of metabolites from *E. siraeum* in positive ion mode, and the lower panel shows the mass spectrum in negative ion mode. The distinct profiles observed in positive and negative ion modes suggest limited overlap in the metabolites detected under these conditions. Figure S5. Functional enrichment analysis of metabolites secreted by *E. siraeum*, based on the number of metabolites in each pathway, revealed significant enrichment in aminoacyl-tRNA biosynthesis, purine metabolism, cysteine and methionine metabolism, arginine and proline metabolism, arginine biosynthesis, tryptophan metabolism, phenylalanine, tyrosine, and tryptophan biosynthesis, glycine, serine, and threonine metabolism, and pyrimidine metabolism. Figure S6. Network relationship between certain metabolites secreted by *Eubacterium siraeum* and functional enrichment pathways. Figure S7. Following oral administration of *Eubacterium siraeum*, significant alterations in host metabolism were observed. OPLS-DA score analysis revealed significant differences between Laiwu pigs and Lulai black pigs. Figure S8. Functional enrichment analysis of the mouse blood metabolites. There are four significantly downregulated metabolic pathways: histidine metabolism, phenylalanine, tyrosine and tryptophan biosynthesis, ubiquinone and other terpenoid-quinone biosynthesis, and phenylalanine metabolism.

Supplementary Material 2: Table S1. The 212 distinct microbes exhibited varying abundances between LW and LL pigs. Table S2. The 198 differentially abundant COGs were identified between LW and LL pigs. Table S3. The 49 differentially abundant blood metabolites were identified between LW and LL pigs. Table S4. The 12 signaling pathways annotated from the 49 differential blood metabolites. Table S5. The Spearman correlation coefficients between 3 feces metabolites and 49 blood metabolites. Table S6. The Spearman correlation coefficients between 4 microbes and 49 blood metabolites. Table S7. The 161 enriched pathways annotated by *Eubacterium siraeum* encode genes. Table S8. The 1,656 metabolites secreted by *Eubacterium siraeum*. Table S9. The differentially abundant fecal metabolites in mice. Table S10. The differentially abundant blood metabolites in mice.

Acknowledgements

We are grateful for the valuable opinions suggested by Dr Huizeng Sun.

Authors' contributions

Qishan Wang and Yuchun Pan conceived this study and provide the financial support. Xueshuang Lai wrote the manuscript. Meng Li collected the samples. Xueshuang Lai, Shuang Liu, Jian Miao, Ran Shen carried out the data analysis. Xueshuang Lai and Shuang Liu depicted the Figs. 1, 2, 3, 4, 5, 6, 7, 8 and supplementary figures. Huanfa Gong provided financial support for the mouse sampling and detected the mouse blood factors. Zhen Wang and Zhe Zhang set up the data analysis process and were mainly looked at raw data sequencing. Qishan Wang, Yuchun Pan, Zhen Wang and Zhe Zhang reviewed and edited the manuscript. All authors have read and approved the final manuscript.

Funding

This work was financially supported by Sanya Science and Technology Innovation Project (2022KJCX49), the Hainan Province Science and Technology Special Fund (ZDYF2024XDNY186), the Zhejiang Science and Technology Major Program on Agricultural New Variety Breeding (2021C02068-1), Shandong Provincial Key R&D Program of China (2021LZGC001) and Zhejiang Provincial Natural Science Foundation of youth project (LQ23C170004).

Data availability

Metagenome sequences data that support the findings of this study have been deposited in the NCBI Sequence Read Archive (SRA) with the accession number PRJNA747893.

Declarations

Ethics approval and consent to participate

All procedures involving the handling of animals included in the pig sampling (license ID: ZJU20220262) and Mouse gavage experiment (license ID: ZJU20230222) were approved by the Institutional Animal Care and Use Committee of Zhejiang University. All experimental methods and experiments were in accordance with the Helsinki Declaration and ARRIVE guidelines.

Consent for publication

Not applicable.

Competing interests

The authors declare no competing interests.

Author details

¹Department of Animal Science, College of Animal Sciences, Zhejiang University, Hangzhou 310030, PR China. ²Hainan Institute, Zhejiang University, Sanya 310014, PR China. ³Jinan Laiwu Pig Industry Technology Research Institute Co., Ltd, Jinan 271100, China.

Received: 2 July 2024 Accepted: 4 October 2024

Published online: 30 October 2024

References

- Fernandez X, Monin G, Talmant A, Mourot J, Lebreton B. Influence of intramuscular fat content on the quality of pig meat - 1. Composition of the lipid fraction and sensory characteristics of *m. longissimus lumborum*. *Meat Sci.* 1999;53(1):59–65.
- Zhou G, Wang S, Wang Z, Zhu X, Shu G, Liao W, Yu K, Gao P, Xi Q, Wang X, et al. Global comparison of gene expression profiles between intramuscular and subcutaneous adipocytes of neonatal landrace pig using microarray. *Meat Sci.* 2010;86(2):440–50.
- Pi-Sunyer FX. The obesity epidemic: pathophysiology and consequences of obesity. *Obes Res.* 2002;10(Suppl 2):97s–104s.
- Sullivan PW, Ghushchyan VH, Ben-Joseph R. The impact of obesity on diabetes, hyperlipidemia and hypertension in the United States. *Qual Life Res.* 2008;17(8):1063–71.
- Khan MT, Nieuwdorp M, Bäckhed F. Microbial modulation of insulin sensitivity. *Cell Metab.* 2014;20(5):753–60.
- Xiong X, Liu X, Zhou L, Yang J, Yang B, Ma H, Xie X, Huang Y, Fang S, Xiao S, et al. Genome-wide association analysis reveals genetic loci and candidate genes for meat quality traits in Chinese Laiwu pigs. *Mamm Genome.* 2015;26(3–4):181–90.
- Qiao R, Gao J, Zhang Z, Li L, Xie X, Fan Y, Cui L, Ma J, Ai H, Ren J, et al. Genome-wide association analyses reveal significant loci and strong candidate genes for growth and fatness traits in two pig populations. *Genet Sel Evol.* 2015;47(1):17.
- Guo Y, Qiu H, Xiao S, Wu Z, Yang M, Yang J, Ren J, Huang L. A genome-wide association study identifies genomic loci associated with backfat thickness, carcass weight, and body weight in two commercial pig populations. *J Appl Genet.* 2017;58(4):499–508.
- Cho IC, Park HB, Ahn JS, Han SH, Lee JB, Lim HT, Yoo CK, Jung EJ, Kim DH, Sun WS, et al. A functional regulatory variant of MYH3 influences muscle fiber-type composition and intramuscular fat content in pigs. *PLoS Genet.* 2019;15(10): e1008279.
- Zilber-Rosenberg I, Rosenberg E. Role of microorganisms in the evolution of animals and plants: the hologenome theory of evolution. *FEMS Microbiol Rev.* 2008;32(5):723–35.
- Yan H, Diao H, Xiao Y, Li W, Yu B, He J, Yu J, Zheng P, Mao X, Luo Y, et al. Gut microbiota can transfer fiber characteristics and lipid metabolic profiles of skeletal muscle from pigs to germ-free mice. *Sci Rep.* 2016;6: 31786.
- Ma J, Duan Y, Li R, Liang X, Li T, Huang X, Yin Y, Yin J. Gut microbial profiles and the role in lipid metabolism in Shaziling pigs. *Anim Nutr.* 2022;9:345–56.

13. Chen C, Fang S, Wei H, He M, Fu H, Xiong X, Zhou Y, Wu J, Gao J, Yang H, et al. *Prevotella copri* increases fat accumulation in pigs fed with formula diets. *Microbiome*. 2021;9(1):175.
14. Krautkrämer KA, Fan J, Bäckhed F. Gut microbial metabolites as multi-kingdom intermediates. *Nat Rev Microbiol*. 2021;19(2):77–94.
15. Li X, Shimizu Y, Kimura I. Gut microbial metabolite short-chain fatty acids and obesity. *Biosci Microbiota Food Health*. 2017;36(4):135–40.
16. Lai X, Zhang Z, Zhang Z, Liu S, Bai C, Chen Z, Qadri QR, Fang Y, Wang Z, Pan Y, et al. Integrated microbiome-metabolome-genome axis data of Laiwu and Lulai pigs. *Sci Data*. 2023;10(1):280.
17. Cao R, Feng J, Xu Y, Fang Y, Zhao W, Zhang Z, Zhang Z, Li M, Wang Q, Pan Y. Genomic signatures reveal breeding effects of Lulai pigs. *Genes (Basel)*. 2022;13(11):1969.
18. Chen QM, Wang H, Zeng YQ, Chen W. Developmental changes and effect on intramuscular fat content of H-FABP and A-FABP mRNA expression in pigs. *J Appl Genet*. 2013;54(1):119–23.
19. Bolger AM, Lohse M, Usadel B. Trimmomatic: a flexible trimmer for Illumina sequence data. *Bioinformatics*. 2014;30(15):2114–20.
20. Li H, Durbin R. Fast and accurate short read alignment with burrows-wheeler transform. *Bioinformatics*. 2009;25(14):1754–60.
21. Peng Y, Leung HC, Yiu SM, Chin FY. IDBA-UD: a de novo assembler for single-cell and metagenomic sequencing data with highly uneven depth. *Bioinformatics*. 2012;28(11):1420–8.
22. Zhu W, Lomsadze A, Borodovsky M. Ab initio gene identification in metagenomic sequences. *Nucleic Acids Res*. 2010;38(12):e132.
23. Li W, Godzik A. Cd-hit: a fast program for clustering and comparing large sets of protein or nucleotide sequences. *Bioinformatics*. 2006;22(13):1658–9.
24. Gu S, Fang L, Xu X. Using SOAPaligner for Short Reads Alignment. *Curr Protoc Bioinform*. 2013;44:11.11.11–17.
25. Galperin MY, Kristensen DM, Makarova KS, Wolf YI, Koonin EV. Microbial genome analysis: the COG approach. *Brief Bioinform*. 2019;20(4):1063–70.
26. Iastrebova OV. Functioning of fructose-1,6-bisphosphatase—main enzyme of gluconeogenesis in microorganisms. *Ukr Biokhim Zh (1999)*. 2002;74(4):24–32.
27. Legouis D, Faivre A, Cippà PE, de Seigneux S. Renal gluconeogenesis: an underestimated role of the kidney in systemic glucose metabolism. *Nephrol Dial Transplant*. 2022;37(8):1417–25.
28. Russell TR, Demeler B, Tu SC. Kinetic mechanism and quaternary structure of *Aminobacter aminovorans* NADH:flavin oxidoreductase: an unusual flavin reductase with bound flavin. *Biochemistry*. 2004;43(6):1580–90.
29. Sáenz de Urturi D, Buqué X, Porteiro B, Folgueira C, Mora A, Delgado TC, Prieto-Fernández E, Olaizola P, Gómez-Santos B, Apodaka-Biguri M, et al. Methionine adenosyltransferase 1a antisense oligonucleotides activate the liver-brown adipose tissue axis preventing obesity and associated hepatosteatosis. *Nat Commun*. 2022;13(1):1096.
30. Isidor MS, Winther S, Markussen LK, Basse AL, Quistorff B, Nedergaard J, Emanuelli B, Hansen JB. Pyruvate kinase M2 represses thermogenic gene expression in brown adipocytes. *FEBS Lett*. 2020;594(7):1218–25.
31. Turnbaugh PJ, Ley RE, Mahowald MA, Magrini V, Mardis ER, Gordon JL. An obesity-associated gut microbiome with increased capacity for energy harvest. *Nature*. 2006;444(7122):1027–31.
32. Sonnenburg JL, Bäckhed F. Diet-microbiota interactions as moderators of human metabolism. *Nature*. 2016;535(7610):56–64.
33. Festi D, Schiumerini R, Eusebi LH, Marasco G, Taddia M, Colecchia A. Gut microbiota and metabolic syndrome. *World J Gastroenterol*. 2014;20(43):16079–94.
34. Toniolo P, Van Kappel AL, Akhmedkhanov A, Ferrari P, Kato I, Shore RE, Riboli E. Serum carotenoids and breast cancer. *Am J Epidemiol*. 2001;153(12):1142–7.
35. Shimode S, Miyata K, Araki M, Shindo K. Antioxidant activities of the antheraxanthin-related carotenoids, antheraxanthin, 9-cis-antheraxanthin, and mutatoxanthins. *J Oleo Sci*. 2018;67(8):977–81.
36. Swargiary G, Mani S. Molecular docking and simulation studies of phyto-compounds derived from *Centella asiatica* and *Andrographis paniculata* against hexokinase II as mitocan agents. *Mitochondrion*. 2021;61:138–46.
37. Daood HG, Palotás G, Palotás G, Somogyi G, Pék Z, Helyes L. Carotenoid and antioxidant content of ground paprika from indoor-cultivated traditional varieties and new hybrids of spice red peppers. *Food Res Int*. 2014;65:231–7.
38. Shen MC, Zhao X, Siegal GP, Desmond R, Hardy RW. Dietary stearic acid leads to a reduction of visceral adipose tissue in athymic nude mice. *PLoS ONE*. 2014;9(9):e104083.
39. Yoneshiro T, Kaede R, Nagaya K, Aoyama J, Saito M, Okamatsu-Ogura Y, Kimura K, Terao A. Royal jelly ameliorates diet-induced obesity and glucose intolerance by promoting brown adipose tissue thermogenesis in mice. *Obes Res Clin Pract*. 2018;12(Suppl 2):127–37.
40. Irandoost P, Mesri Alamdari N, Saidpour A, Shidfar F, Roshanravan N, Asghari Jafarabadi M, Farsi F, Asghari Hanjani N, Vafa M. The effects of royal jelly and tocotrienol-rich fraction on impaired glycemic control and inflammation through irisin in obese rats. *J Food Biochem*. 2020;44(12):e13493.
41. Keppley LJW, Walker SJ, Gademsey AN, Smith JP, Keller SR, Kester M, Fox TE. Nervous acid limits weight gain in a mouse model of diet-induced obesity. *Faseb j*. 2020;34(11):15314–26.
42. Park YK, Obiang-Obounou BW, Lee J, Lee TY, Bae MA, Hwang KS, Lee KB, Choi JS, Jang BC. Anti-Adipogenic Effects on 3T3-L1 Cells and Zebrafish by Tanshinone IIA. *Int J Mol Sci*. 2017;18(10):2065.
43. Raz I, Eldor R, Cernea S, Shafir E. Diabetes: insulin resistance and derangements in lipid metabolism. Cure through intervention in fat transport and storage. *Diabetes Metab Res Rev*. 2005;21(1):3–14.
44. Martínez-Sánchez N. There and back again: leptin actions in white adipose tissue. *Int J Mol Sci*. 2020;21(17):6039.
45. Trayhurn P. Adipokines: inflammation and the pleiotropic role of white adipose tissue. *Br J Nutr*. 2022;127(2):161–4.
46. Dang TTH, Yun JW. Cytochrome P450 2E1 (CYP2E1) positively regulates lipid catabolism and induces browning in 3T3-L1 white adipocytes. *Life Sci*. 2021;278:119648.
47. Abdelmegeed MA, Choi Y, Godlewski G, Ha SK, Banerjee A, Jang S, Song BJ. Cytochrome P450–2E1 promotes fast food-mediated hepatic fibrosis. *Sci Rep*. 2017;7:39764.
48. Nguyen Huu T, Park J, Zhang Y, Park I, Yoon HJ, Woo HA, Lee SR. Redox Regulation of PTEN by Peroxiredoxins. *Antioxidants (Basel)*. 2021;10(2):302.
49. Chiarugi P, Cirri P. Redox regulation of protein tyrosine phosphatases during receptor tyrosine kinase signal transduction. *Trends Biochem Sci*. 2003;28(9):509–14.
50. Yin Y, Huang X, Lynn KD, Thorpe PE. Phosphatidylserine-targeting antibody induces M1 macrophage polarization and promotes myeloid-derived suppressor cell differentiation. *Cancer Immunol Res*. 2013;1(4):256–68.
51. Dai W, Zhang J, Chen L, Yu J, Zhang J, Yin H, Shang Q, Yu G. Discovery of *Bacteroides uniformis* F18–22 as a Safe and Novel Probiotic Bacterium for the Treatment of Ulcerative Colitis from the Healthy Human Colon. *Int J Mol Sci*. 2023;24(19):14669.
52. Qiao X, Gao Y, Li J, Wang Z, Qiao H, Qi H. Sensitive analysis of single nucleotide variation by Cas13d orthologs, *EsCas13d* and *RspCas13d*. *Biotechnol Bioeng*. 2021;118(8):3037–45.
53. Wang Y, Wang Y, Tang N, Wang Z, Pan D, Ji Q. Characterization and engineering of a novel miniature eubacterium *Siraeum* CRISPR-Cas12f System. *ACS Synth Biol*. 2024;13(7):2115–27.
54. Yan WX, Chong S, Zhang H, Makarova KS, Koonin EV, Cheng DR, Scott DA. Cas13d Is a compact RNA-targeting Type VI CRISPR effector positively modulated by a WYL-domain-containing accessory protein. *Mol Cell*. 2018;70(2):327–339.e325.
55. Hu X, Yu C, He Y, Zhu S, Wang S, Xu Z, You S, Jiao Y, Liu SL, Bao H. Integrative metagenomic analysis reveals distinct gut microbial signatures related to obesity. *BMC Microbiol*. 2024;24(1):19.
56. Newman TM, Shively CA, Register TC, Appt SE, Yadav H, Colwell RR, Fanelli B, Dadlani M, Graubics K, Nguyen UT, et al. Diet, obesity, and the gut microbiome as determinants modulating metabolic outcomes in a non-human primate model. *Microbiome*. 2021;9(1):100.
57. Ye D, Huang J, Wu J, Xie K, Gao X, Yan K, Zhang P, Tao Y, Li Y, Zang S, et al. Integrative metagenomic and metabolomic analyses reveal gut microbiota-derived multiple hits connected to development of gestational diabetes mellitus in humans. *Gut Microbes*. 2023;15(1):2154552.
58. Wang M, Xu X, Sheng M, Zhang M, Wu F, Zhao Z, Guo M, Fang B, Wu J. Tannic acid protects against colitis by regulating the IL17 - NFκB and microbiota - methylation pathways. *Int J Biol Macromol*. 2024;274(Pt 1):133334.
59. Zhao N, Ma Y, Liang X, Zhang Y, Hong D, Wang Y, Bai D. Efficacy and Mechanism of Qianshan Huoxue Gao in Acute Coronary Syndrome via Regulation of Intestinal Flora and Metabolites. *Drug Des Devel Ther*. 2023;17:579–95.

60. Zhu Z, Hu C, Liu Y, Wang F, Zhu B. Inulin has a beneficial effect by modulating the intestinal microbiome in a BALB/c mouse model. *Benef Microbes*. 2023;14(4):371–83.
61. He J, Zhang P, Shen L, Niu L, Tan Y, Chen L, Zhao Y, Bai L, Hao X, Li X, et al. Short-chain fatty acids and their association with signalling pathways in inflammation, glucose and lipid metabolism. *Int J Mol Sci*. 2020;21(17):6356.
62. den Besten G, van Eunen K, Groen AK, Venema K, Reijngoud DJ, Bakker BM. The role of short-chain fatty acids in the interplay between diet, gut microbiota, and host energy metabolism. *J Lipid Res*. 2013;54(9):2325–40.
63. Du J, Zhang P, Luo J, Shen L, Zhang S, Gu H, He J, Wang L, Zhao X, Gan M, et al. Dietary betaine prevents obesity through gut microbiota-driven microRNA-378a family. *Gut Microbes*. 2021;13(1):1–19.
64. Sahuri-Arisoylu M, Brody LP, Parkinson JR, Parkes H, Navaratnam N, Miller AD, Thomas EL, Frost G, Bell JD. Reprogramming of hepatic fat accumulation and “browning” of adipose tissue by the short-chain fatty acid acetate. *Int J Obes (Lond)*. 2016;40(6):955–63.
65. Ye RZ, Richard G, Gérvy N, Tchernof A, Carpentier AC. Fat cell size: measurement methods, pathophysiological origins, and relationships with metabolic dysregulations. *Endocr Rev*. 2022;43(1):35–60.
66. Ikeda K, Yamada T. UCP1 dependent and independent thermogenesis in brown and beige adipocytes. *Front Endocrinol (Lausanne)*. 2020;11:498.
67. Viladomiu M, Hontecillas R, Bassaganya-Riera J. Modulation of inflammation and immunity by dietary conjugated linoleic acid. *Eur J Pharmacol*. 2016;785:87–95.
68. Muhammad I, Luo W, Shoaib RM, Li GL, Shams UI Hassan S, Yang ZH, Xiao X, Tu GL, Yan SK, Ma XP, et al. Guaiane-type sesquiterpenoids from *Cinnamomum migao* H. W. Li: And their anti-inflammatory activities. *Phytochemistry*. 2021;190: 112850.
69. Li HM, Fan M, Xue Y, Peng LY, Wu XD, Liu D, Li RT, Zhao QS. Guaiane-Type Sesquiterpenoids from *Alismatis Rhizoma* and Their Anti-inflammatory Activity. *Chem Pharm Bull (Tokyo)*. 2017;65(4):403–7.
70. Guo R, Duan ZK, Li Q, Yao GD, Song SJ, Huang XX. Guide isolation of guaiane-type sesquiterpenoids from *Daphne tangutica maxim*. And their anti-inflammatory activities. *Phytochemistry*. 2023;206:113523.
71. Matsubara K, Matsuzawa Y, Jiao S, Kihara S, Takama T, Nakamura T, Tokunaga K, Kubo M, Tarui S. Cholesterol-lowering effect of N-(alpha-methylbenzyl)linoleamide (melinamide) in cholesterol-fed diabetic rats. *Atherosclerosis*. 1988;72(2–3):199–204.
72. Nakajima T, Natori K, Hirohashi T, Aono S. Inhibitory effect of melinamide on cholesterol solubility in mixed micellar solution of sodium taurocholate. *Chem Pharm Bull (Tokyo)*. 1986;34(10):4273–9.
73. Barcenilla A, Pryde SE, Martin JC, Duncan SH, Stewart CS, Henderson C, Flint HJ. Phylogenetic relationships of butyrate-producing bacteria from the human gut. *Appl Environ Microbiol*. 2000;66(4):1654–61.
74. Louis P, Flint HJ. Formation of propionate and butyrate by the human colonic microbiota. *Environ Microbiol*. 2017;19(1):29–41.
75. Turrioni S, Rampelli S, Biagi E, Consolandi C, Severgnini M, Peano C, Quercia S, Soverini M, Carbonero FG, Bianconi G, et al. Temporal dynamics of the gut microbiota in people sharing a confined environment, a 520-day ground-based space simulation, MARS500. *Microbiome*. 2017;5(1):39.
76. Inoki K, Li Y, Zhu T, Wu J, Guan KL. TSC2 is phosphorylated and inhibited by Akt and suppresses mTOR signalling. *Nat Cell Biol*. 2002;4(9):648–57.
77. Degirmenci U, Wang M, Hu J. Targeting Aberrant RAS/RAF/MEK/ERK Signaling for Cancer Therapy. *Cells*. 2020;9(1):198.
78. Savova MS, Mihaylova LV, Tews D, Wabitsch M, Georgiev MI. Targeting PI3K/AKT signaling pathway in obesity. *Biomed Pharmacother*. 2023;159: 114244.
79. Feng H, Liu T, Yousuf S, Zhang X, Huang W, Li A, Xie L, Miao X. Identification and analysis of lncRNA, miRNA and mRNA related to subcutaneous and intramuscular fat in Laiwu pigs. *Front Endocrinol (Lausanne)*. 2022;13:1081460.
80. Feng H, Yousuf S, Liu T, Zhang X, Huang W, Li A, Xie L, Miao X. The comprehensive detection of miRNA and circRNA in the regulation of intramuscular and subcutaneous adipose tissue of Laiwu pig. *Sci Rep*. 2022;12(1):16542.
81. Feng H, Liu TY, Salsabeel Y, Miao XY. Transcriptome analysis of intramuscular and subcutaneous fat of Laiwu pig. *Life Sci Res*. 2023;27(02):179–88.

Publisher's Note

Springer Nature remains neutral with regard to jurisdictional claims in published maps and institutional affiliations.